AD-A 086 096

AD A086096

MEMORANDUM REPORT ARBRL-MR-03019
(Supersedes IMR No. 637)

AERODYNAMIC CHARACTERISTICS OF THE 30MM, XM788 PROJECTILE

Robert L. McCoy

May 1980

US ARMY ARMAMENT RESEARCH AND DEVELOPMENT COMMAND
BALLISTIC RESEARCH LABORATORY
ABERDEEN PROVING GROUND, MARYLAND

UNCLASSIFIED

SECURITY CLASSIFICATION OF THIS PAGE (When Data Entered)

REPORT DOCUMENTATION PAGE		READ INSTRUCTIONS BEFORE COMPLETING FORM
1. REPORT NUMBER MEMORANDUM REPORT ARBRL-MR-03019	2. GOVT ACCESSION NO.	3. RECIPIENT'S CATALOG NUMBER
4. TITLE (and Subtitle) AERODYNAMIC CHARACTERISTICS OF THE 30MM, XM788 PROJECTILE		5. TYPE OF REPORT & PERIOD COVERED Final
		6. PERFORMING ORG. REPORT NUMBER
7. AUTHOR(s) Robert L. McCoy		8. CONTRACT OR GRANT NUMBER(s)
9. PERFORMING ORGANIZATION NAME AND ADDRESS U.S. Army Ballistic Research Laboratory (ATTN: DRDAR-BLL) Aberdeen Proving Ground, MD 21005		10. PROGRAM ELEMENT, PROJECT, TASK AREA & WORK UNIT NUMBERS RDT&E 1X4642070425
11. CONTROLLING OFFICE NAME AND ADDRESS U.S. Army Armament Research & Development Command U.S. Army Ballistic Research Laboratory (ATTN: DRDAR-BL) Aberdeen Proving Ground, MD 21005		12. REPORT DATE May 1980
		13. NUMBER OF PAGES 50
14. MONITORING AGENCY NAME & ADDRESS(if different from Controlling Office)		15. SECURITY CLASS. (of this report) Unclassified
		15a. DECLASSIFICATION/DOWNGRADING SCHEDULE

16. DISTRIBUTION STATEMENT (of this Report)

Approved for public release, distribution unlimited

17. DISTRIBUTION STATEMENT (of the abstract entered in Block 20, if different from Report)

18. SUPPLEMENTARY NOTES

This report supersedes IMR 637, March 1979.

19. KEY WORDS (Continue on reverse side if necessary and identify by block number)

30mm XM788 Projectile
Aerodynamic Characteristics
Aerodynamic Drag and Stability
Yaw Limit-Cycle

20. ABSTRACT (Continue on reverse side if necessary and identify by block number) ner/ajb

Spark range tests of the 30mm, XM788 projectile were conducted to determine the small-yaw aerodynamic properties at supersonic, transonic, and subsonic speeds. The XM788 projectile, fired from the XM230E1 barrel is adequately gyroscopically stable at all speeds tested. The data show that a slow-arm (precession) limit-cycle yaw exists at low transonic and subsonic speeds. The drag increase due to the limit-cycle yaw is discussed.

TABLE OF CONTENTS

LIST OF ILLUSTRATIONS

LIST OF TABLES

I. INTRODUCTION

On 27 January 1978, a meeting was held at Hughes Helicopters, Culver City, California, to discuss the technical characteristics of the 30mm ammunition for the Chain Gun. Personnel from the Project Manager, Advanced Attack Helicopter (PM-AAH), the Ballistic Research Laboratory (BRL), and Hughes Helicopters (HH) were present. One of the results of the meeting was a joint recommendation to fire a fifteen (15) round program of 30mm, XM788 Target Practice (TP) projectiles through the BRL Aerodynamics Range, to obtain basic aerodynamic data. The ammunition was to be provided by Honeywell, Inc. (subcontractor to HH), HH was to provide the gun, and the PM-AAH agreed to fund the BRL test.

The 30mm barrel for testing was received from HH in April 1978, and thirty (30) rounds of XM788 TP ammunition in a separate shipment. The XM788 test was placed on the firing schedule at BRL. On 11 May 1978, word was received from the PM-AAH that the projectiles sent to BRL had defective rotating bands, and should be returned to the contractor. New projectiles were received mid-October 1978. The BRL test was rescheduled, and firing began on 15 November 1978.

II. TEST PROCEDURE

All tests were conducted in the BRL Aerodynamics Range[1]. Physical measurements were made, utilizing the methods described in Reference 2 for dimensions, weights, and centers of mass. The axial and transverse moments of inertia were obtained to within ±0.03% error, using the recently acquired equipment from Space Electronics Corporation. The average physical characteristics of the test projectiles are included in Figure 1, which shows the dimensional details. Figure 2 is a photograph of the XM788 TP projectile.

The test rounds were fired from a 30mm Mann barrel, No. 387-7025, S/N11, with a constant twist rate (6° 30'). Various propellants and charge weights were selected to achieve the required test Mach numbers. A half-muzzle type yaw inducer was used for one round (Test Round No. 13477), to investigate the effects of large yaw at a Mach number around 0.8; all other rounds were launched without yaw induction.

---

1. *W. F. Braun, "The Free Flight Aerodynamics Range," Ballistic Research Laboratories Report No. 1048, August 1958. AD 202249.*

2. *E. R. Dickinson, "Physical Measurements of Projectiles," Ballistic Research Laboratories Technical Note No. 874, February 1954, AD 803103.*

All test rounds were equipped with a single pin installed near the outer edge of the base, to provide highly accurate spin measurements. In addition to the fifteen (15) round program, two warmer rounds (13463 and 13464) also provided useful data. The warmer rounds were not equipped with roll pins, so no spin damping was obtained from these two flights. The rotating bands of rounds 13478 and 13479 were pre-engraved, to reduce shot-start pressure at very low loading density. Round number 13478, which was intended to be a second data point at Mach number 0.6, failed to launch properly, and was lost. The data obtained from the sixteen (16) successful flights are presented in this report.

III. RESULTS

The range data were fitted to solutions of the linearized equation of motion and these results used to infer linearized aerodynamic coefficients, using the methods of Reference 3. The actual projectile aerodynamic force-moment system often is not strictly linear. Given sufficient data the actual non-linear behavior can be determined from the range results[4]. For the 30mm XM788 projectiles, sufficient data were obtained to permit determination of some non-linear aerodynamic coefficients. A more detailed analysis of non-linear effects is presented in the various subtopics of this section, which discuss individual aerodynamic coefficients.

A useful by-product of tests conducted in the BRL aerodynamics ranges is the high quality shadowgraph information obtained. Figures 3 through 10 show the flowfield around the 30mm, XM788 projectiles, at speeds ranging from supersonic down to high subsonic. Figures 3 through 9 were selected for locally small yaw (angle of attack less than 1/2 degree). Figure 10 shows the XM788 projectile at an angle of attack of 7.7 degrees, and Mach number of 0.84. Boundary layer separation on the leeward side of the projectile is evident in Figure 10.

The round-by-round aerodynamic data obtained is listed in Table I, and flight motion parameters are given in Table II.

---

3. *C. H. Murphy, "Data Reduction for the Free Flight Spark Ranges," Ballistic Research Laboratories Report No. 900, February 1954, AD 35833.*

4. *C. H. Murphy, "The Measurement of Non-Linear Forces and Moments by Means of Free Flight Tests," Ballistic Research Laboratories Report No. 974, February 1956, AD 93521.*

A. Drag Coefficient

The drag coefficient, C_D, is determined by fitting the time-distance measurements from the range flight. C_D is distinctly non-linear with yaw level, and the value determined from an individual flight reflects both the zero-yaw drag coefficient, C_{D_o}, and the induced drag due to the average yaw level of the flight. The drag coefficient variation is expressed as an even power series in yaw amplitude:

$$C_D = C_{D_o} + C_{D_{\delta^2}}\delta^2 + C_{D_{\delta^4}}\delta^4 + \ldots.$$

where C_{D_o} is the zero-yaw drag coefficient, $C_{D_{\delta^2}}$ and $C_{D_{\delta^4}}$ are the quadratic and quartic yaw-drag coefficients, and δ^2 is the total angle of attack squared.

For the 30mm, XM788 projectile, only the quadratic yaw-drag coefficient, $C_{D_{\delta^2}}$, and the zero-yaw drag coefficient, C_{D_o} could be determined for supersonic speeds, since the average yaw levels for the supersonic flights ranged from 0.5 degree to 3.5 degrees. At subsonic speeds, one round (No. 13477) was fired with a yaw-inducer to obtain 8 degrees angle of attack, and the data from this flight, combined with the other subsonic drag data allowed a determination of both $C_{D_{\delta^2}}$ and $C_{D_{\delta^4}}$. The yaw-drag coefficients for the various regimes were then used to correct the range values of C_D to zero-yaw conditions.

Figure 11 shows the variation of C_{D_o} with Mach number. Figure 12 is a plot of the quadratic yaw-drag coefficient, $C_{D_{\delta^2}}$, versus Mach number. Insufficient data were obtained at transonic speeds to permit determination of $C_{D_{\delta^2}}$; hence the dashed line on Figure 12 was used to connect the subsonic and supersonic regions. Figure 13 shows the variation of total drag coefficient, C_D, with angle of attack at subsonic speeds.

B. Spin Damping Moment Coefficient

The spin damping moment coefficient, C_{ℓ_p}, is determined by fitting roll angle-distance measurements from the range. Variation of C_{ℓ_p}

with yaw level is usually much weaker than that observed for the drag coefficient, and in the present tests, no significant variation of C_{ℓ_p} with yaw could be determined. Figure 14 is a plot of C_{ℓ_p} versus Mach number for the 30mm, XM788 projectile.

C. Pitching Moment Coefficient

The range values of the pitching moment coefficient, C_{M_α}, were fitted using the appropriate squared-yaw parameter from Reference 4. C_{M_α} was found to vary significantly with yaw level at supersonic speeds; the subsonic dependence of C_{M_α} with yaw was much weaker. The pitching moment is assumed to be cubic in yaw level, and the coefficient variation is given by:

$$C_{M_\alpha} = C_{M_{\alpha_o}} + C_2\delta^2$$

where $C_{M_{\alpha_o}}$ is the zero-yaw pitching moment coefficient, and C_2 is the cubic coefficient.

For the 30mm, XM788 projectile, the value of C_2 at supersonic speeds was found to be -16. The subsonic value of C_2 was -0.5. The cubic coefficients were used to correct the range values of C_{M_α} to zero-yaw conditions, and Figure 15 shows the variation of $C_{M_{\alpha_o}}$ with Mach number.

D. Gyroscopic Stability

The 30mm, XM788 projectile has ample launch gyroscopic stability when fired at standard velocity (805 metres/second) from the 6° 30' twist rate (27.57 calibers/turn) of the XM230E1 barrel. The average launch gyroscopic stability factor (S_g) of the four rounds launched at standard conditions is 3.17. Since the XM788 is never fired at reduced velocities, and the ratio of axial spin to forward velocity increases continuously for flat trajectories, the slightly lower values of S_g observed in Table II for the lower Mach numbers will never occur in field firings.

The XM788 projectile is designed to be launched in forward fire from an aircraft. The addition of the aircraft's velocity vector to the gun muzzle velocity has the effect of reducing the projectile's launch gyroscopic stability factor by the ratio:

$$\left(\frac{V_{Muzzle}}{V_{A/C} + V_{Muzzle}}\right)^2$$

The following table shows the effect of aircraft speed on launch S_g, for the XM788 in forward fire.

$V_{A/C}$ (Knots)	S_g (Launch)
0	3.17
150	2.64
300	2.23

At an aircraft speed of 300 knots, the XM788, fired from the XM230E1 barrel still has more than adequate gyroscopic stability.

E. Lift Force Coefficient

The lift force coefficient, C_{L_α}, was also analyzed by the method of Reference 4. If the lift force is assumed to be cubic in yaw level, the coefficient variation is given by:

$$C_{L_\alpha} = C_{L_{\alpha_o}} + a_2 \delta^2$$

where $C_{L_{\alpha_o}}$ is the zero-yaw lift force coefficient, and a_2 is the cubic coefficient.

At supersonic speeds, a value of 21 was obtained for a_2; at subsonic speeds the corresponding value was 7. The two values of a_2 were used to correct the range values of C_{L_α} to zero-yaw conditions.

Figure 16 shows the variation of $C_{L_{\alpha_o}}$ with Mach number.

The lift force coefficient is not as well determined from spark range tests as is C_{M_α}. This fact is reflected in the larger round-to-round data scatter observed in Figure 16, compared to the pitching moment data plotted in Figure 15.

F. Magnus Moment Coefficient and Pitch Damping Moment Coefficient

The Magnus moment coefficient, $C_{M_{p\alpha}}$, and the Pitch Damping Moment Coefficient, $(C_{M_q} + C_{M_{\dot{\alpha}}})$, are discussed together, since if either coefficient is non-linear with yaw level, both coefficients exhibit non-linear coupling in the data reduction process[4]. Due to mutual reaction, the analysis of $C_{M_{p\alpha}}$ and $(C_{M_q} + C_{M_{\dot{\alpha}}})$ must be performed simultaneously, although the aerodynamic moments are not, in themselves, directly physically related.

If the dependence of both the Magnus moment and the Pitch Damping moment are cubic in yaw level, the non-linear variation of the two moment coefficients is of the general form:

$$C_{M_{p\alpha}} = C_{M_{p\alpha_o}} + \hat{C}_2\delta^2$$

$$(C_{M_q} + C_{M_{\dot{\alpha}}}) = (C_{M_q} + C_{M_{\dot{\alpha}}})_o + d_2\delta^2$$

where $C_{M_{p\alpha_o}}$ and $(C_{M_q} + C_{M_{\dot{\alpha}}})_o$ are the zero-yaw values of Magnus and Pitch Damping moment coefficients, respectively, and $\hat{C}_2$ and d_2 are the associated cubic coefficients.

In Reference 4 it is shown that the non-linear coupling introduced through the data reduction yields the following expressions for range values [R-subscript] of $C_{M_{p\alpha}}$ and $(C_{M_q} + C_{M_{\dot{\alpha}}})$:

$$[C_{M_{p\alpha}}]_R = C_{M_{p\alpha_o}} + \hat{C}_2\,\delta_e^2 + d_2\,\delta_{e_{TH}}^{\;2}$$

$$[C_{M_q} + C_{M_{\dot\alpha}}]_R = (C_{M_q} + C_{M_{\dot\alpha}})_o + \hat{C}_2\,\delta_{e_{HT}}^{\;2} + d_2\,\delta_{e_{HH}}^{\;2}$$

where the above effective squared yaws are defined as:

$$\delta_e^{\;2} = K_F^{\;2} + K_S^{\;2} + (\phi'_F K_F^{\;2} - \phi'_S K_S^{\;2})/(\phi'_F - \phi'_S)$$

$$\delta_{e_{TH}}^{\;2} = (I_x/I_y)[(K_F^{\;2}\phi'_F{}^2 - K_S^{\;2}\phi'_S{}^2)/(\phi'_F{}^2 - \phi'_S{}^2)]$$

$$\delta_{e_{HT}}^{\;2} = (I_y/I_x)(\phi'_F + \phi'_S)\ (K_S^{\;2} - K_F^{\;2})/(\phi'_F - \phi'_S)$$

$$\delta_{e_{HH}}^{\;2} = (\phi'_F\ K_S^{\;2} - \phi'_S\ K_F^{\;2})/(\phi'_F - \phi'_S)$$

The remaining symbols are defined in the List of Symbols in this report.

Preliminary analysis of the XM788 data indicated that significant values of both $\hat{C}_2$ and d_2 exist for this projectile. Subsequent analysis determined that $[C_{M_{p\alpha}}]_R$ varied significantly with $\delta_e^{\;2}$, but only very weakly with $\delta_{eTH}^{\;2}$, while $[C_{M_q} + C_{M_{\dot\alpha}}]_R$ showed a strong dependence on both non-linear terms. Hence, the Magnus moment data was fitted assuming a dependence on $\delta_e^{\;2}$ only, and values were obtained for $\hat{C}_2$ at subsonic and supersonic speeds. Using the known values of $\hat{C}_2$, the Pitch Damping data was re-analyzed to determine improved values of d_2.

The values finally obtained for $\hat{C}_2$ and c_2 are given below:

Mach Region	$\hat{C}_2$	d_2
Subsonic	29	-224
Supersonic	48	-224

The above tabulated values for $\hat{C}_2$ and d_2 were used to correct the range values of $C_{M_{p\alpha}}$ and $(C_{M_q} + C_{M_{\dot{\alpha}}})$ to zero-yaw conditions. Figure 17 is a plot of $C_{M_{p\alpha_o}}$ versus Mach number, and Figure 18 is a similar plot of $(C_{M_q} + C_{M_{\dot{\alpha}}})$.

It should be noted that the analysis of non-linear Magnus and Pitch Damping data from free flight spark ranges is a delicate process at best; i.e., the results are highly sensitive to small errors in determination of the damping exponents on the two modal arms. In view of this fact, the $C_{M_{p\alpha}}$ and $(C_{M_q} + C_{M_{\dot{\alpha}}})$ analysis of this report should be regarded with some suspicion, at the least, until such time as computed flight dynamic behavior for the XM788 can be verified by a long-range flight-dynamic experiment.

G. Damping Rates

The damping rates, λ_F and λ_S, of the fast and slow yaw modes indicate the dynamic stability of a projectile. Negative λ's indicate damping; a positive λ means that its associated modal arm will grow with increasing time.

For a projectile whose Magnus or Pitch Damping moments are cubic with yaw level, the damping rates also show a non-linear dependence on yaw[4]. The cubic variation of the damping rates can be written:

$$\lambda_F = \lambda_{F_o} + \lambda_{F_2} (K_F^2 + 2K_S^2)$$

$$\lambda_S = \lambda_{S_o} + \lambda_{S_2} (2K_F^2 + K_S^2)$$

The damping rates for the 30mm, XM788 projectile were analyzed using the above equations, and values obtained for λ_{F_2} and λ_{S_2} at subsonic and supersonic speeds are given below:

Mach Region	λ_{F_2}	λ_{S_2}
Subsonic	-.0039	-.0112
Supersonic	+.0047	-.0203

The above tabulated values were used to correct the range values of λ_F and λ_S to zero-yaw conditions. Figures 19 and 20 show the zero-yaw behavior of the fast and slow arm damping rates at various Mach numbers.

Figure 19 shows that between flight Mach numbers of 0.65 to 0.85, the fast arm damping rate is slightly positive, for very small yaw levels. However, the cubic coefficient, λ_{F_2}, is negative in this region, indicating that increasing yaw level will decrease the size of the positive λ_{F_o}. Hence, a small fast arm limit cycle could exist, in a relatively narrow band of flight Mach numbers.

Figure 20 shows a wide band of slow arm undamping at zero yaw, for all flight Mach numbers below 1.05. Since the cubic coefficient for λ_S is also negative, a slow arm limit cycle would be expected, and due to relative sizes of terms, both the growth rate and the limit cycle values of the slow arm should exceed that of the fast arm.

The effect of non-linear damping rates can be predicted using the amplitude plane methods of Reference 5. However, a more direct method, which also accounts for damping rate variations with Mach number, is to numerically solve the following system of equations:

$$\frac{d\ K_F^{\ 2}}{ds} = 2\ \lambda_F\ K_F^{\ 2}$$

---

5. *C. H. Murphy, "Free Flight Motion of Symmetric Missiles," Ballistic Research Laboratories Report No. 1216, July 1963, AD 442757.*

$$\frac{d\,K_S^2}{d\,s} = 2\,\lambda_S K_S^2$$

$$\lambda_F = \lambda_{F_o} + \lambda_{F_2}\,(K_F^2 + 2\,K_S^2)$$

$$\lambda_S = \lambda_{S_o} + \lambda_{S_2}\,(2K_F^2 + K_S^2)$$

where s is arc length along the trajectory, and the Mach number variation of the damping rate coefficients is input as a table in arc length.

The 30mm, XM788 projectile is normally launched at a Mach number of 2.3, and for the entire supersonic flight, both damping rates are negative, for all likely yaw levels. Hence, the projectile will normally arrive at transonic speeds with very small yaw, due to the damping of any initial transients. A preliminary calculation showed that at $M_\infty = 1.0$ (approximately 980 metres from the gun), a slow arm amplitude of 0.1 degree and a fast arm amplitude of 0.05 degree would be physically reasonable, and these values were used as initial conditions to start the numerical integration. The Mach number variation with arc length was obtained from a standard trajectory program, using the zero-yaw drag coefficient curve of Figure 11.

The numerical solution of the equations for modal amplitudes showed that the fast arm does not grow to a limit cycle value; in fact, it decreases below the very small initial value assumed, and remains small throughout the subsonic trajectory. The slow arm does reach a limit cycle value, which grows to a magnitude of nearly 4 degrees at a Mach number of 0.70, and then begins to damp as the projectile speed continues to drop. The predicted behavior of the slow arm amplitude at transonic and subsonic speeds is shown in Figure 21.

IV. CONCLUSIONS

The 30mm, XM788 projectile, when launched at a muzzle velocity of 805 metres/second from the XM230E1 barrel, is gyroscopically stable in either forward or side fire, from aircraft speeds in excess of 300 knots.

The spark range data show that a slow-arm (precession) limit-cycle yaw exists at low transonic and subsonic speeds. The magnitude of the limit-cycle varies between three and four degrees, and will

produce a drag increase of between ten and fifteen percent over the zero-yaw value, at subsonic speeds. Since the XM788 reaches transonic speed at around one kilometre range, the drag penalty due to the limit-cycle will affect the trajectory in increasing amounts as the range increases beyond one kilometre. The magnitude of the effect is currently under investigation, using the BRL six-degree-of-freedom program[6], and the aerodynamic data presented in this report.

V. RECOMMENDATIONS

It is recommended that a long-range flight-dynamic experiment be conducted, to verify the predicted subsonic limit-cycle behavior of the XM788 projectile. The flight dynamic experiment should be conducted using the HH Chain Gun (rather than a Mann barrel), and the flight dynamic information could best be provided using the 30mm yawsonde fuze currently under development at the BRL.

Preliminary six-degree-of-freedom calculations indicate a high sensitivity of the trajectory to the magnitude of the first maximum yaw. Due to the effect of weapon dynamics, the distribution of first maximum yaw of projectiles fired from the Chain Gun may be significantly different from that obtained with a Mann barrel. Therefore, it is also recommended that a test be conducted to define the first maximum yaw distribution of XM788 projectiles fired from the Chain Gun.

---

6. *R. F. Lieske and R. L. McCoy, "Equations of Motion of a Rigid Projectile," Ballistic Research Laboratories Report No. 1244, March 1964, AD 441598.*

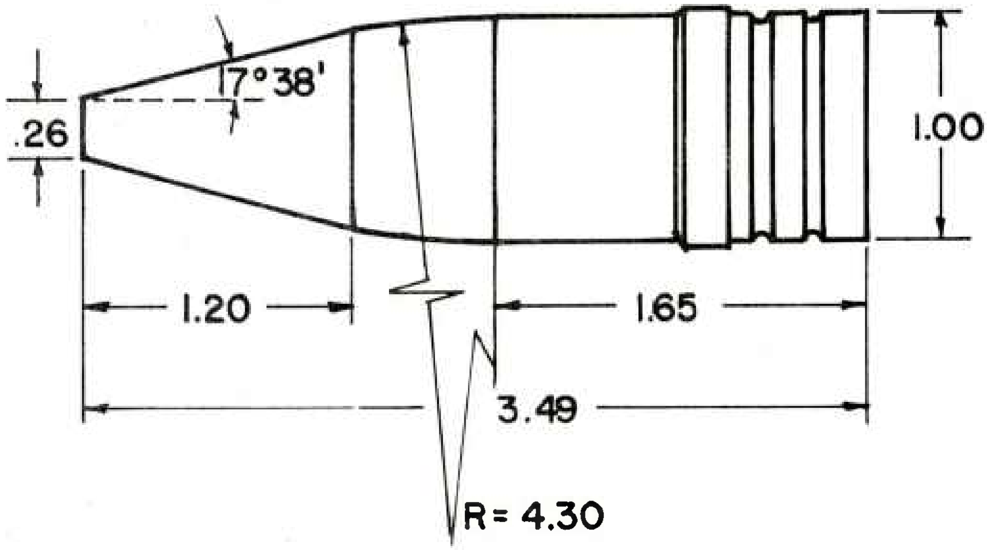

ALL DIMENSIONS IN CALIBERS

(1 CALIBER = 29.92 MM)

WT. = 232.8 gms

C.G. = 1.25 CAL. FROM BASE

I_x = 326.9 gm-cm^2

I_y = 1685 gm-cm^2

Figure 1. Sketch of 30mm, XM788 Projectile

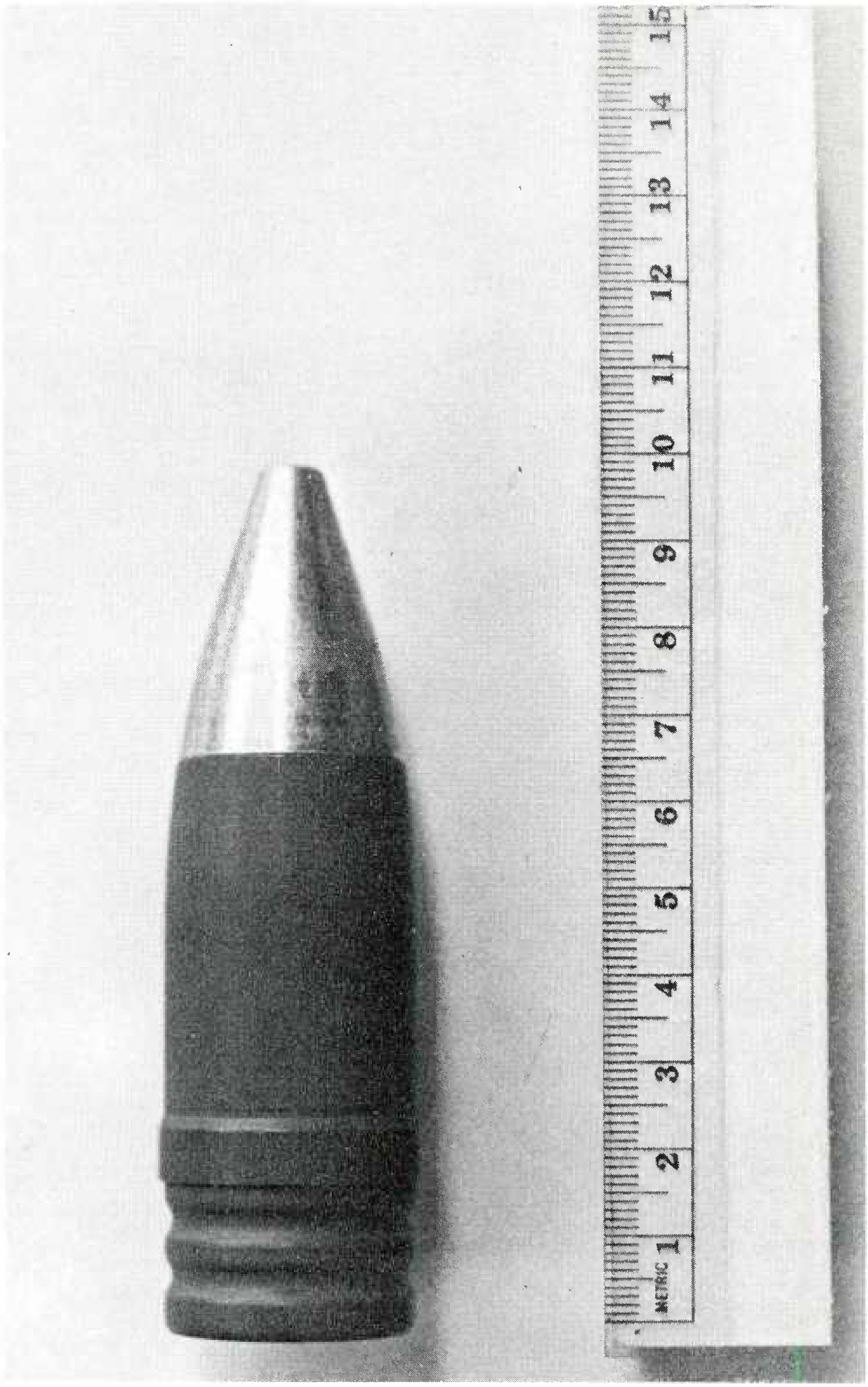

Figure 2. Photograph of 30mm, XM788 Projectile

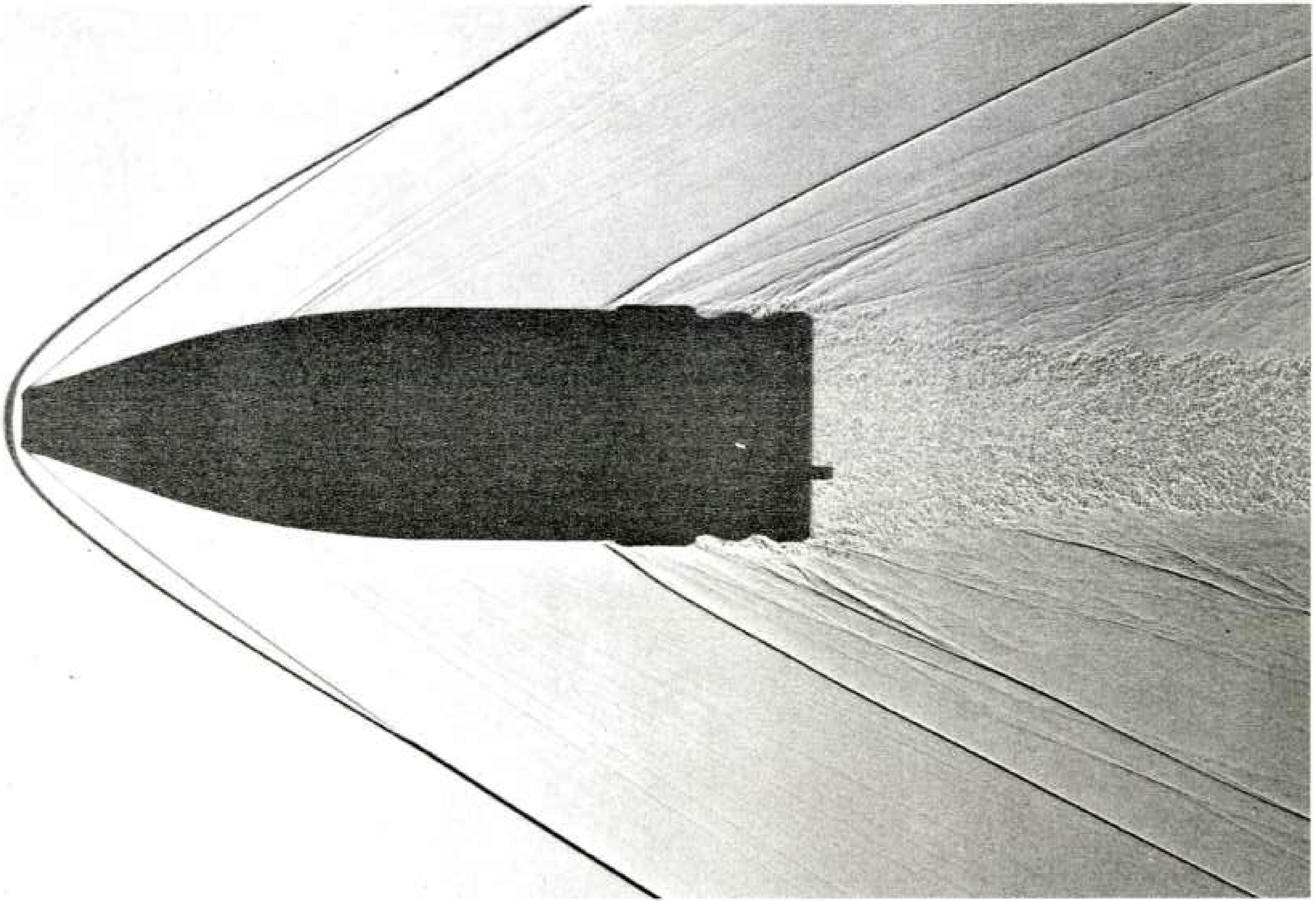

Figure 3. Shadowgraph of XM788 Projectile in Flight at Mach 2.29

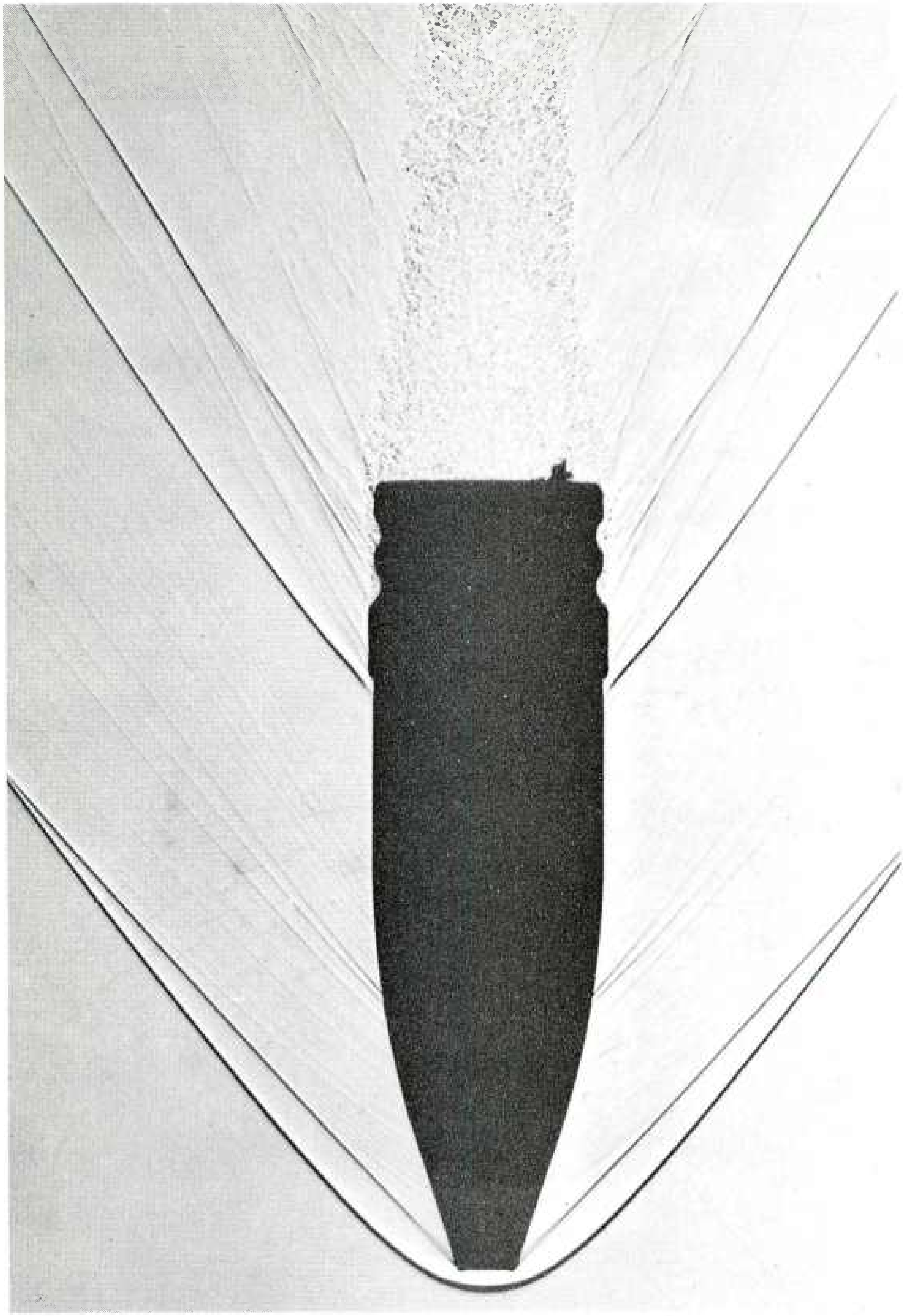

Figure 4. Shadowgraph of XM788 Projectile in Flight at Mach 1.83

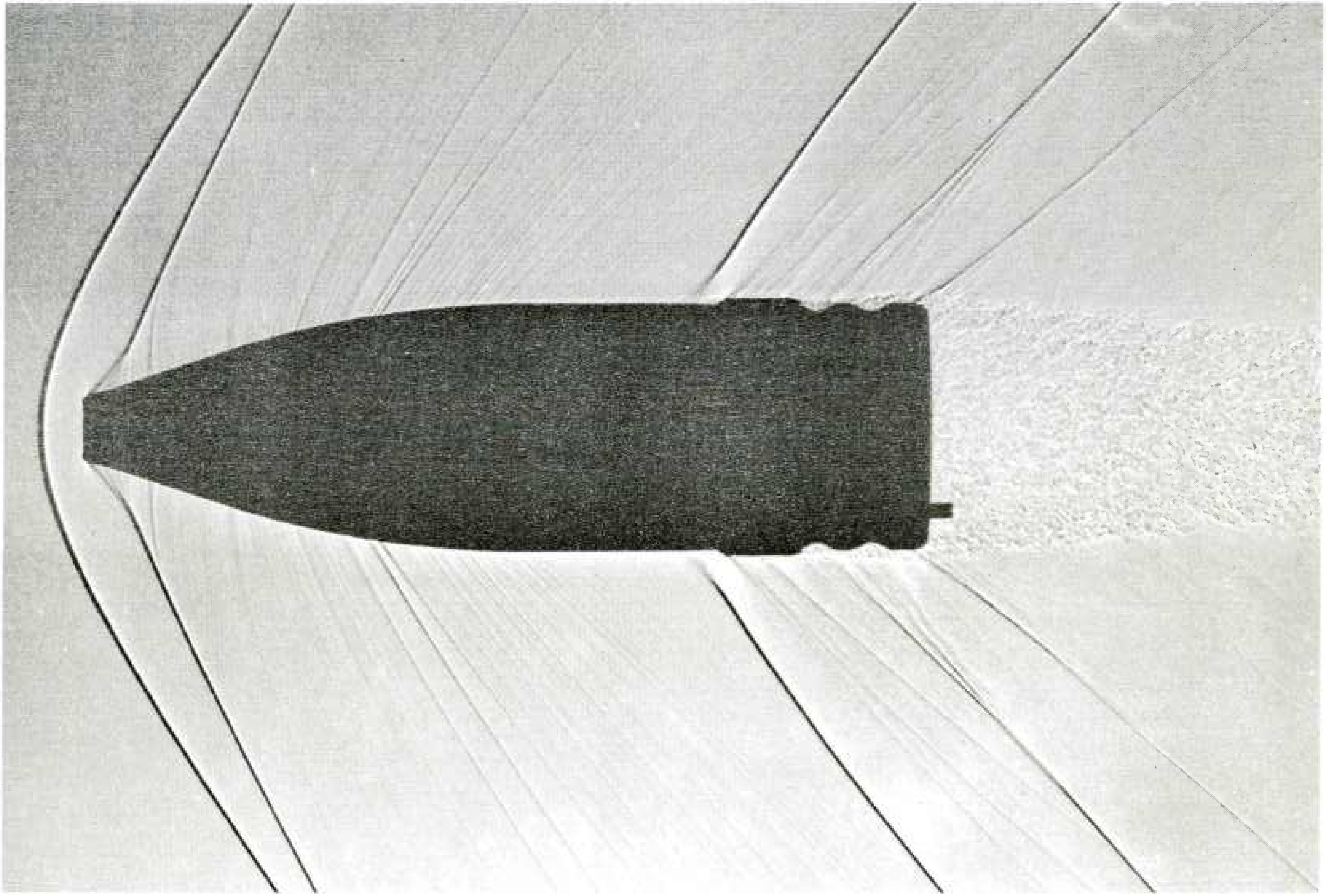

Figure 5. Shadowgraph of XM788 Projectile in Flight at Mach 1.29

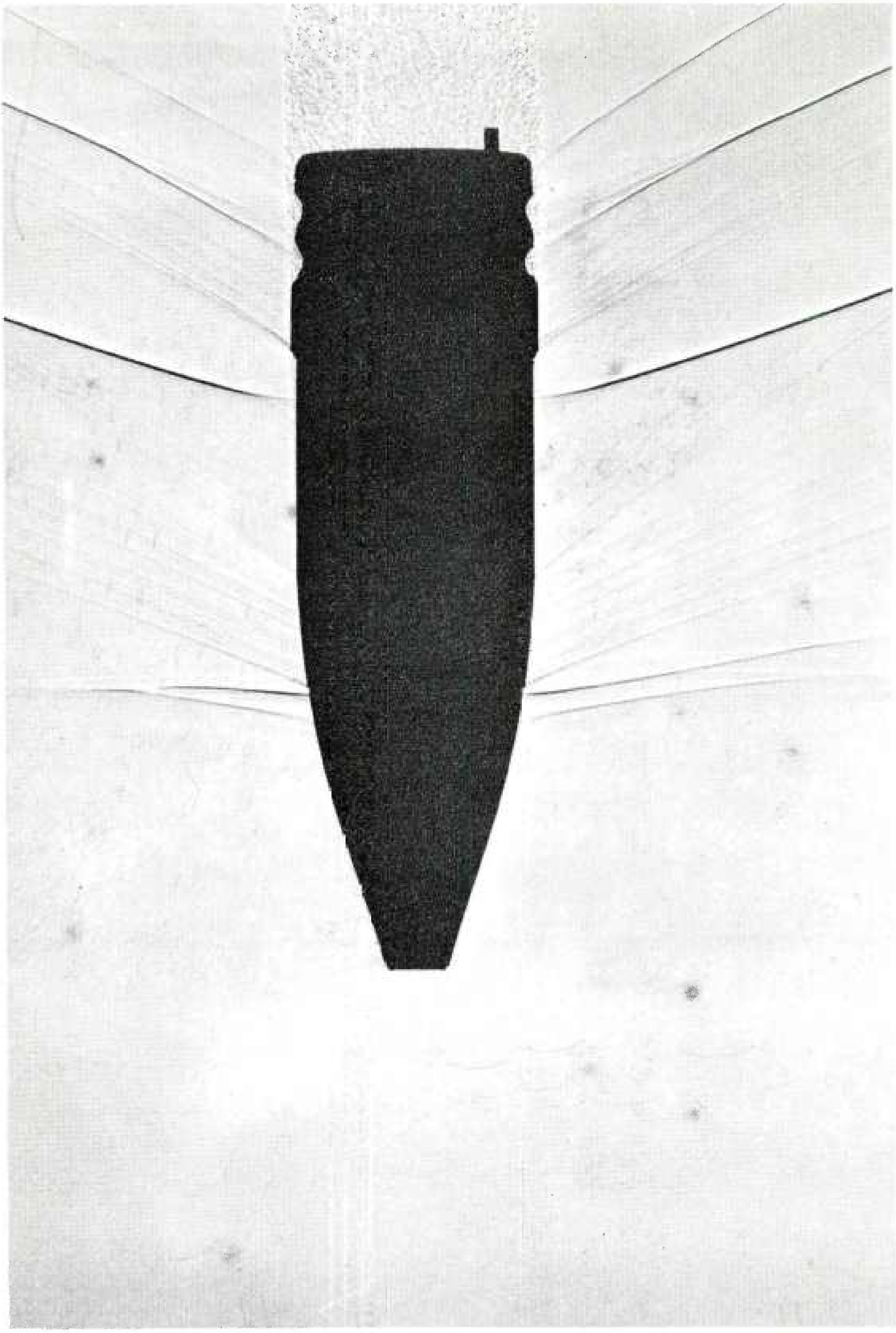

Figure 6. Shadowgraph of XM788 Projectile in Flight at Mach 1.01

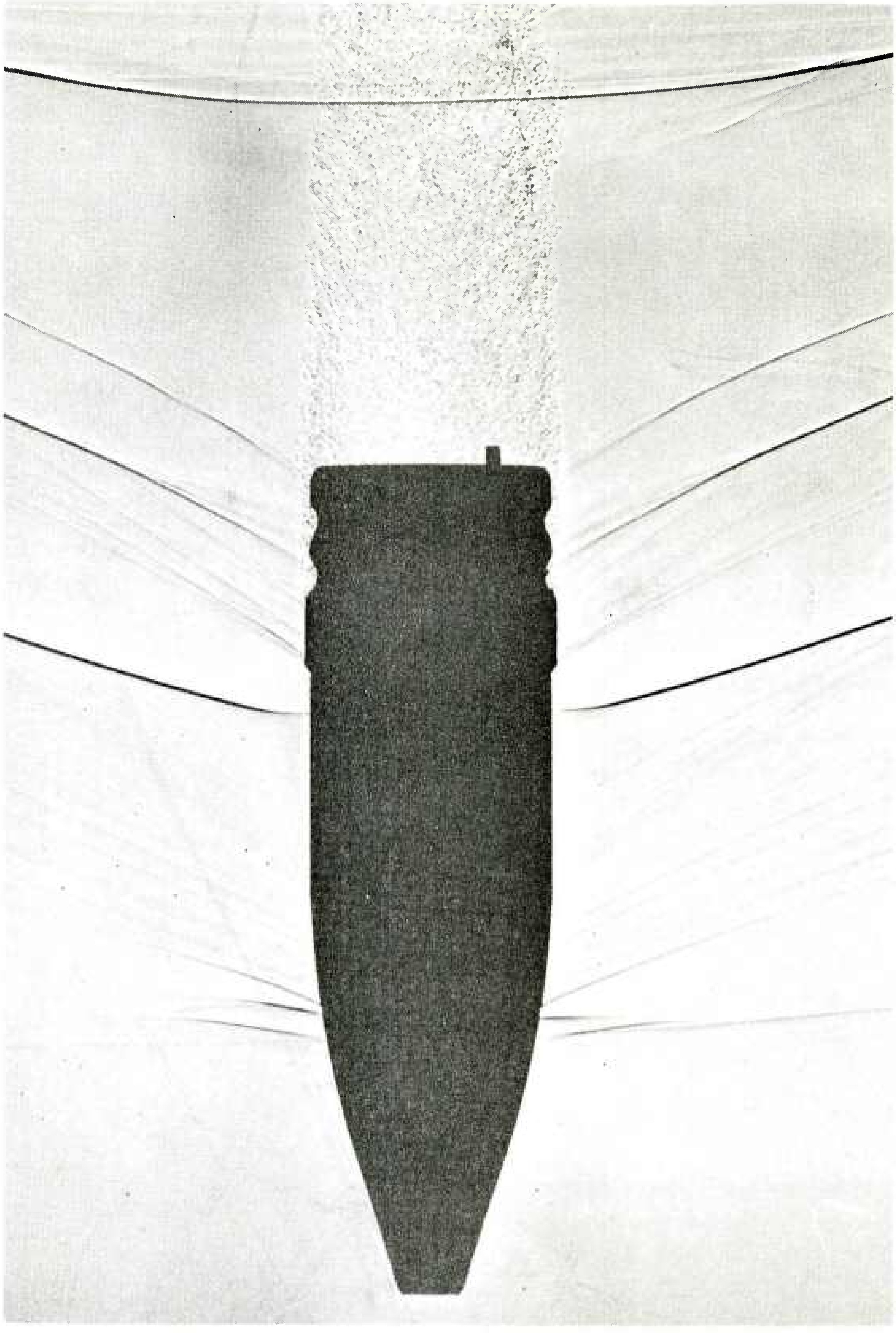

Figure 7. Shadowgraph of XM788 Projectile in Flight at Mach 1.00

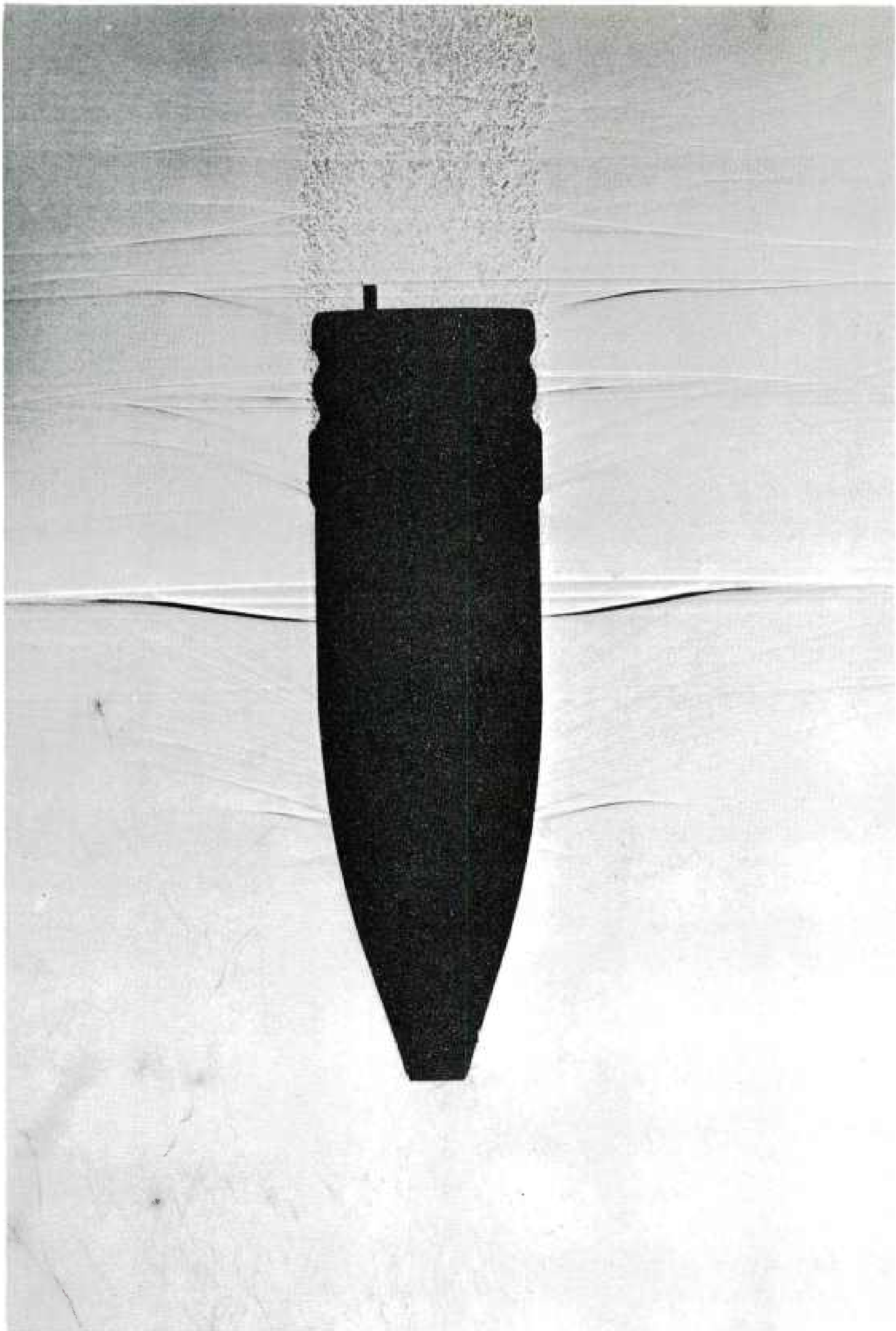

Figure 8. Shadowgraph of XM788 Projectile in Flight at Mach 0.94

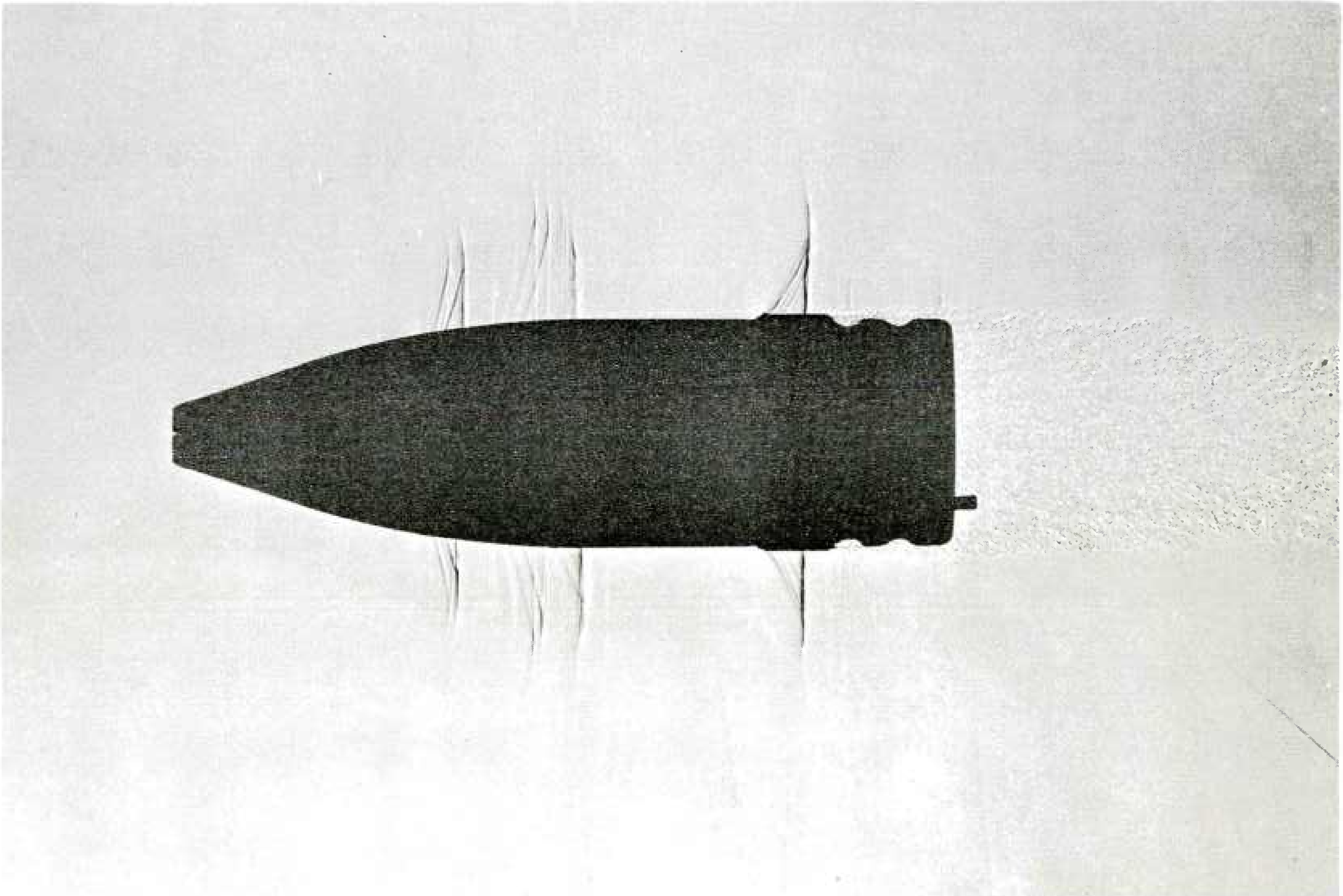

Figure 9. Shadowgraph of XM788 Projectile in Flight at Mach 0.90

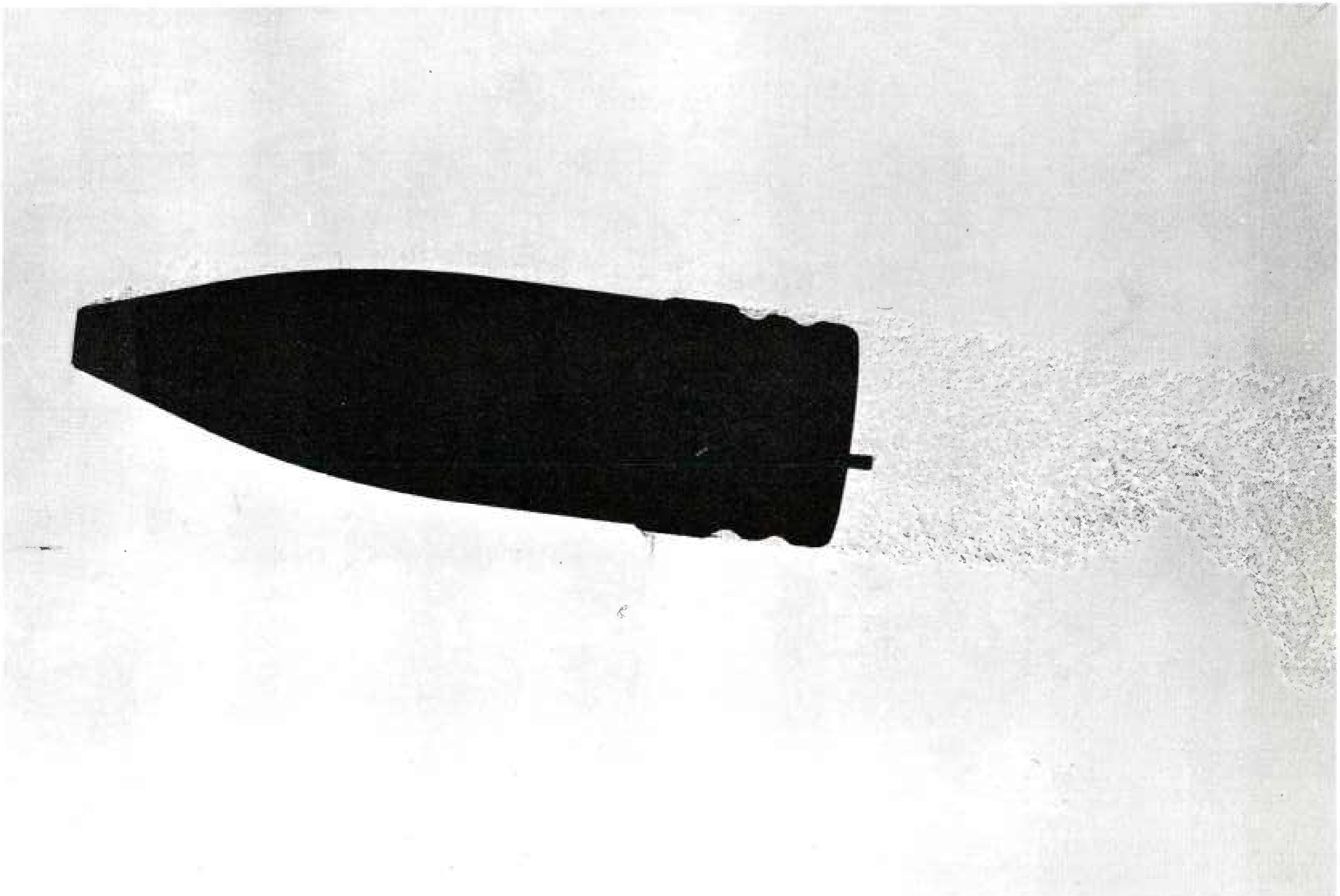

Figure 10. Shadowgraph of XM788 Projectile in Flight at Mach 0.84, angle of attack = 7.7 degrees

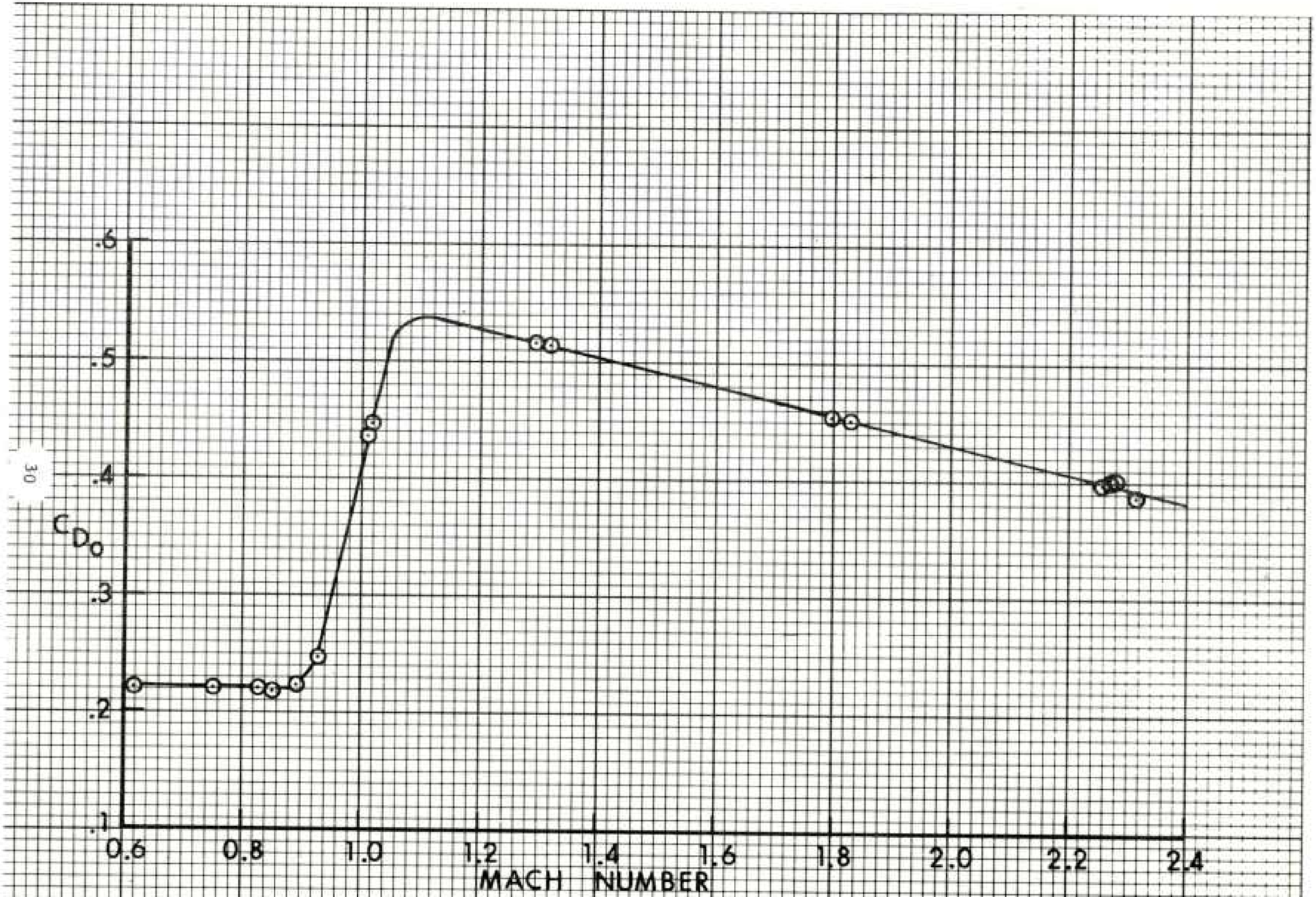

Figure 11. Zero-Yaw Drag Force Coefficient versus Mach Number

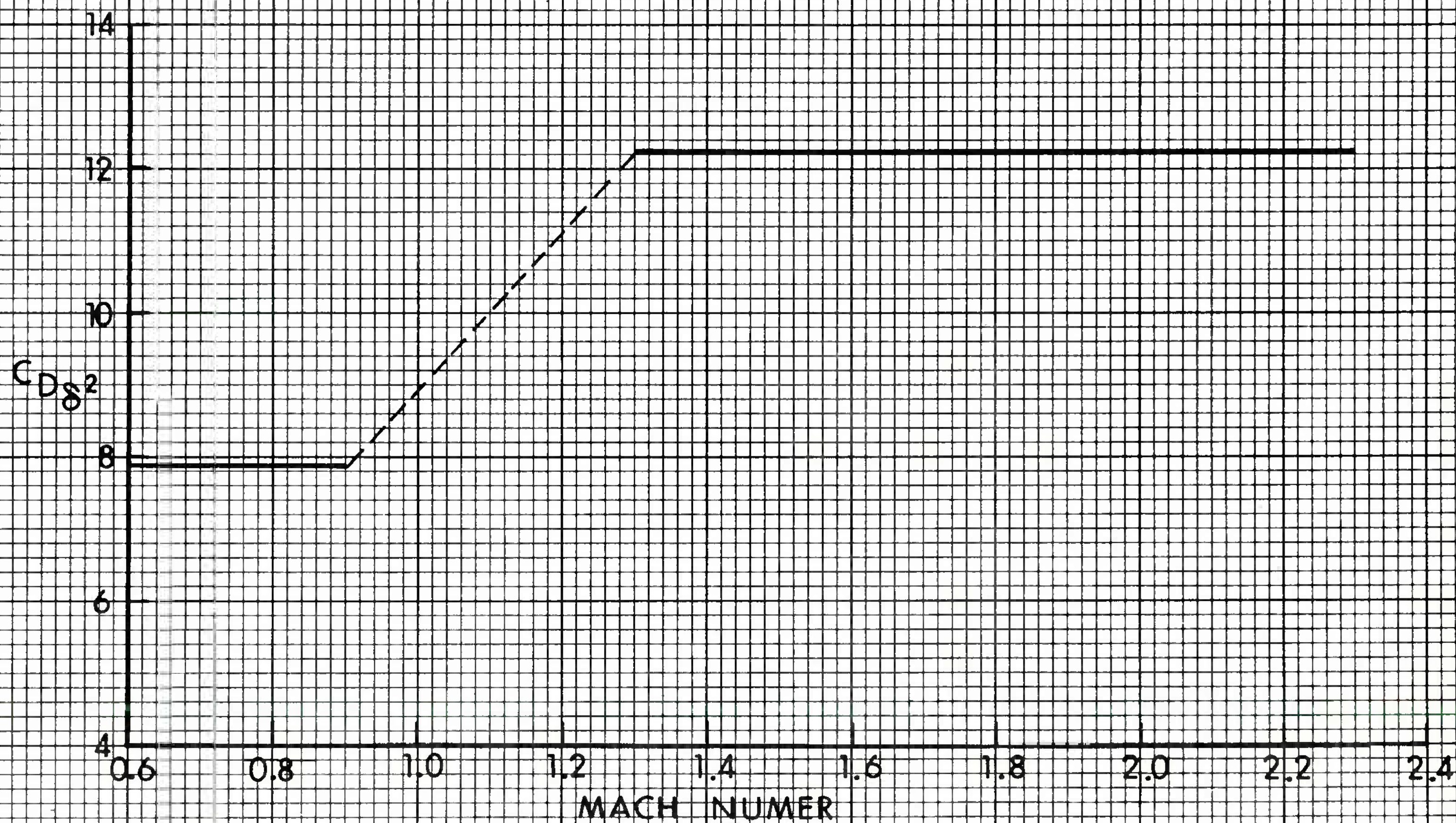

Figure 12. Quadratic Yaw Drag Force Coefficient versus Mach Number

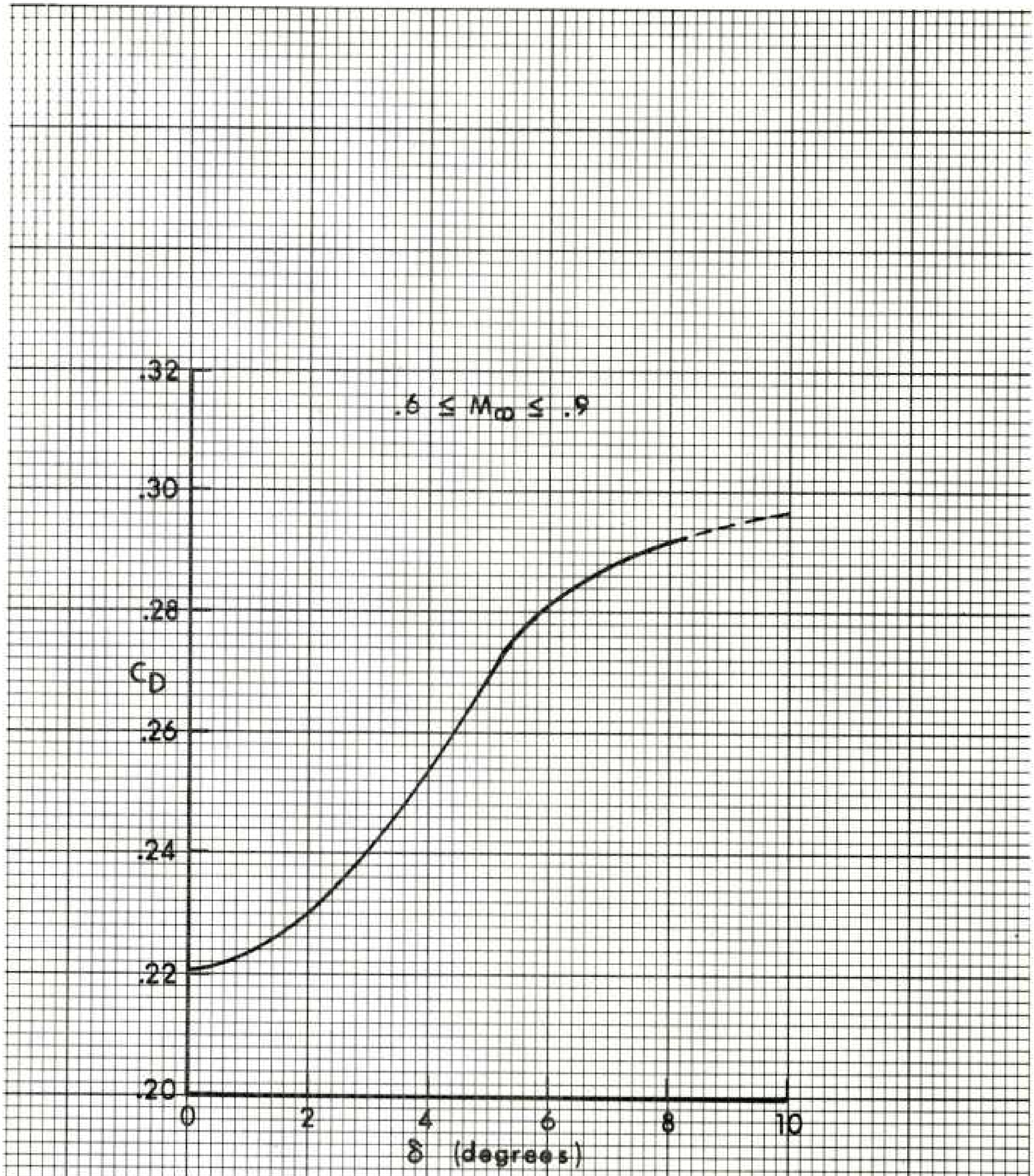

Figure 13. Drag Force Coefficient versus Yaw at Subsonic Speeds

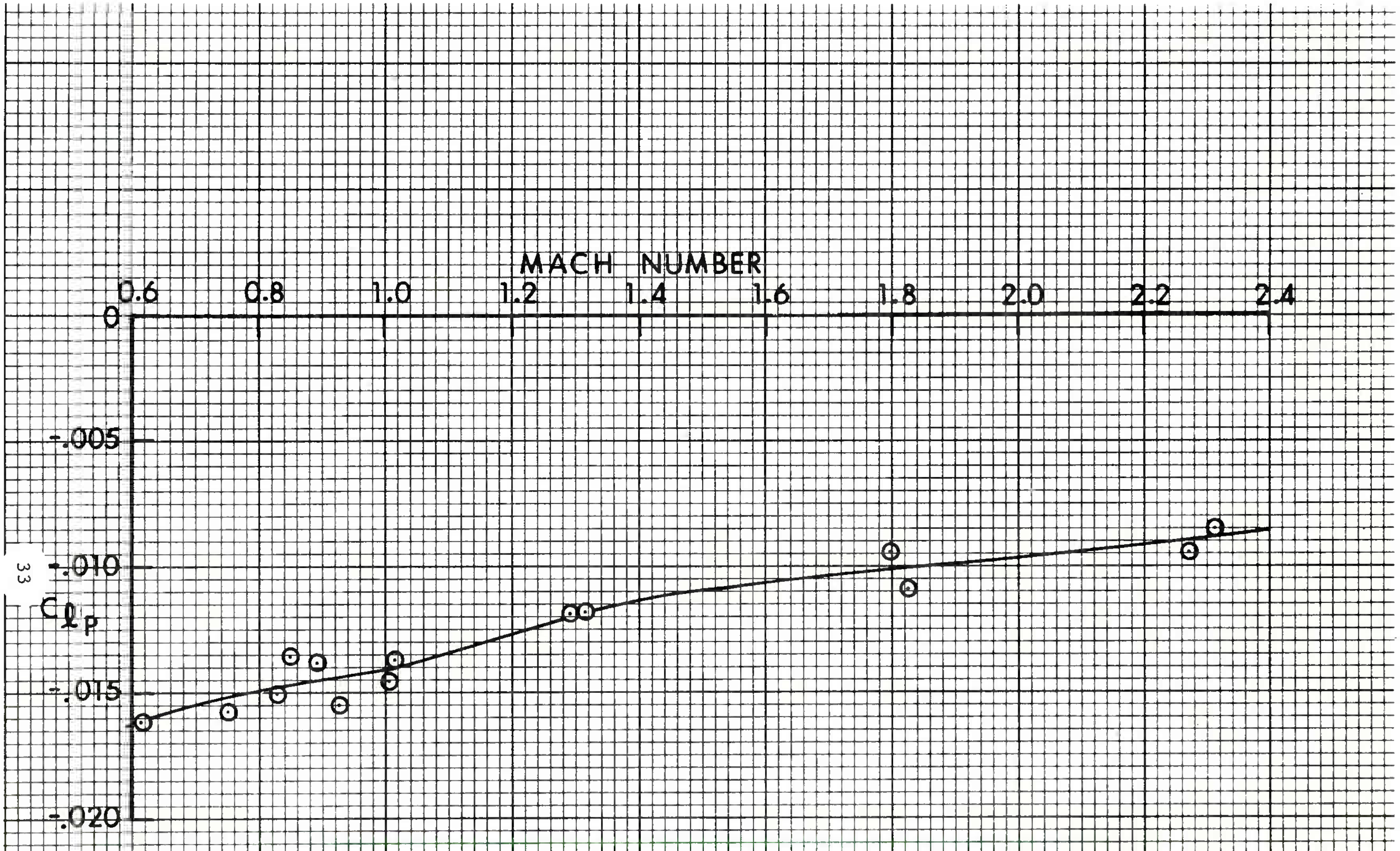

Figure 14. Spin Damping Moment Coefficient versus Mach Number

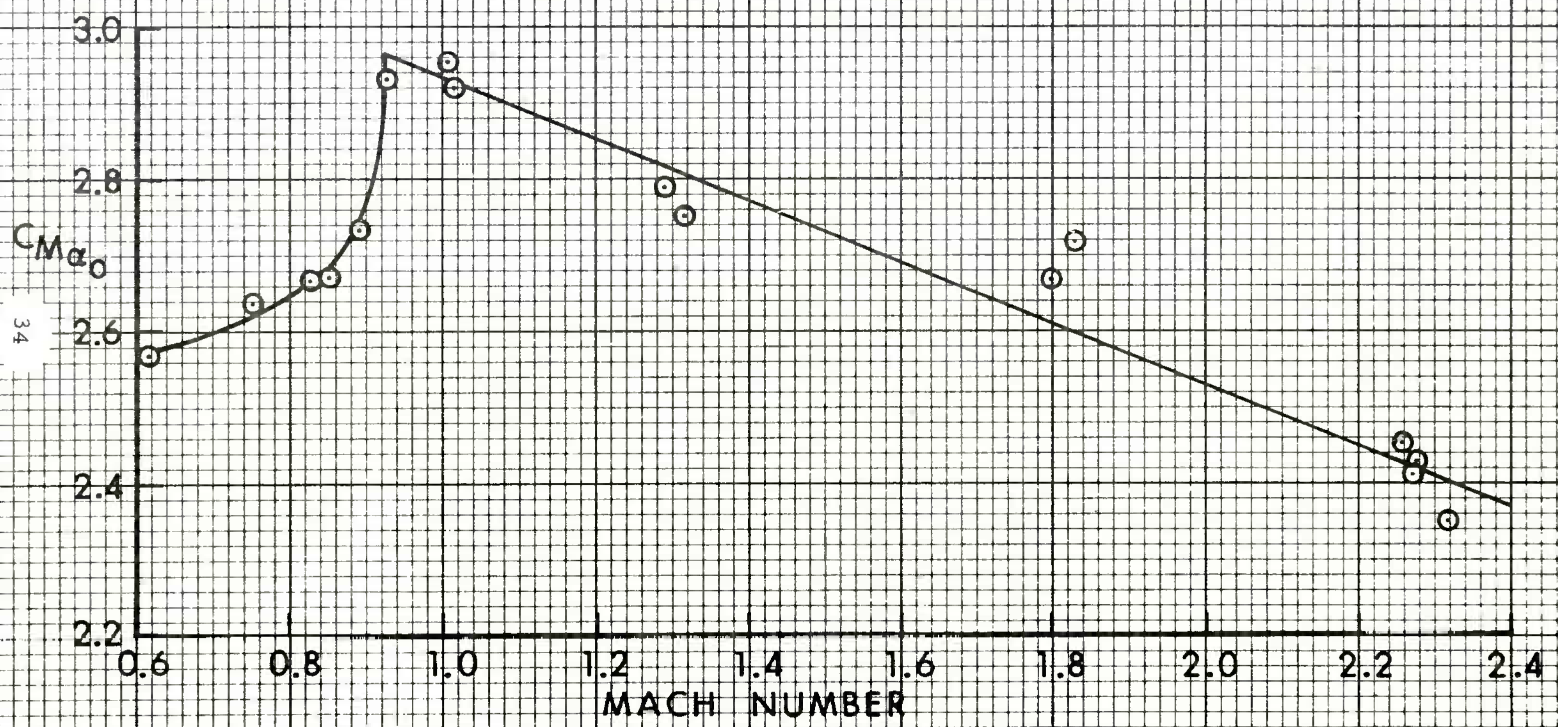

Figure 15. Zero-Yaw Pitching Moment Coefficient versus Mach Number

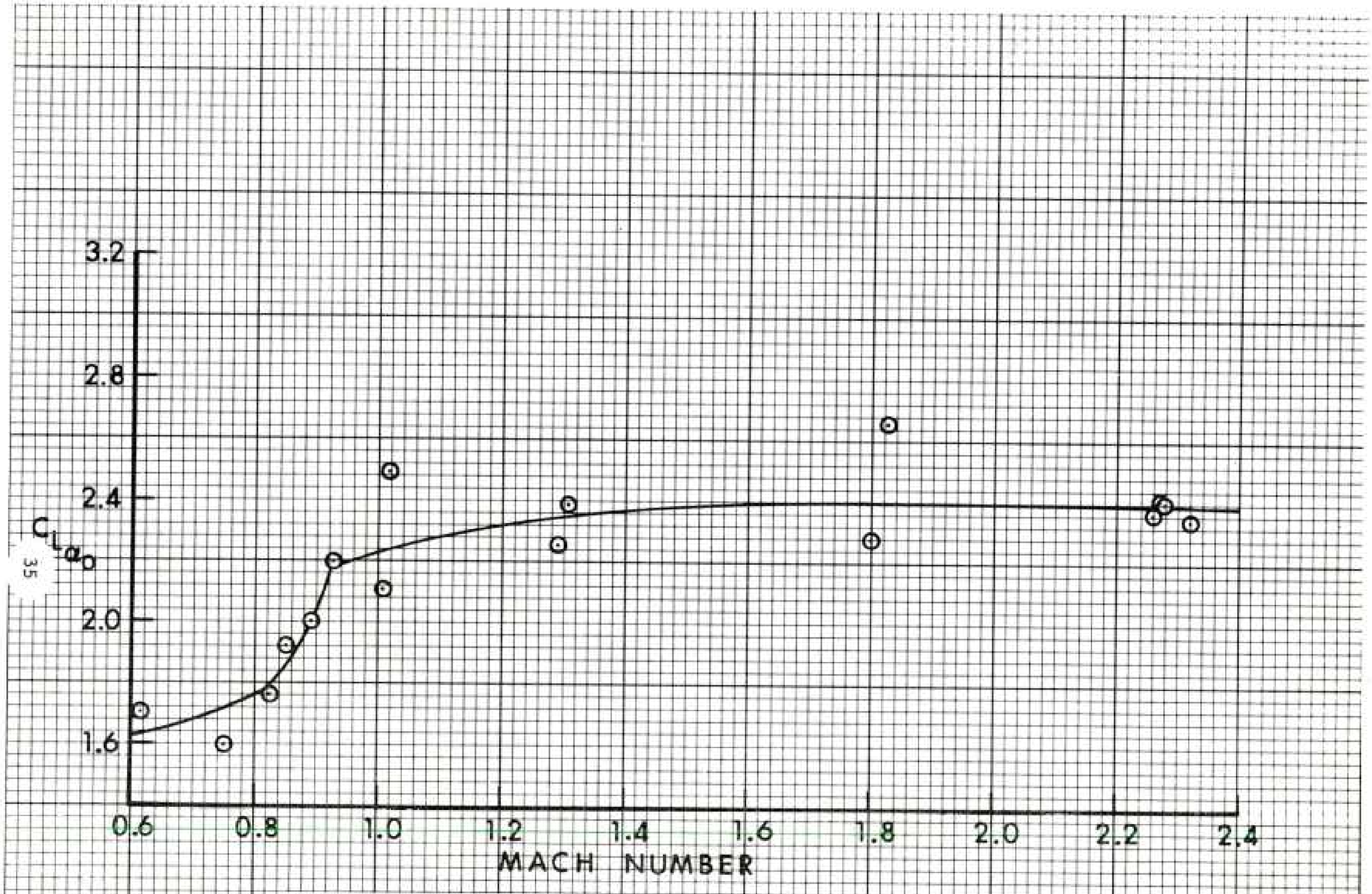

Figure 16. Zero-Yaw Lift Force Coefficient versus Mach Number

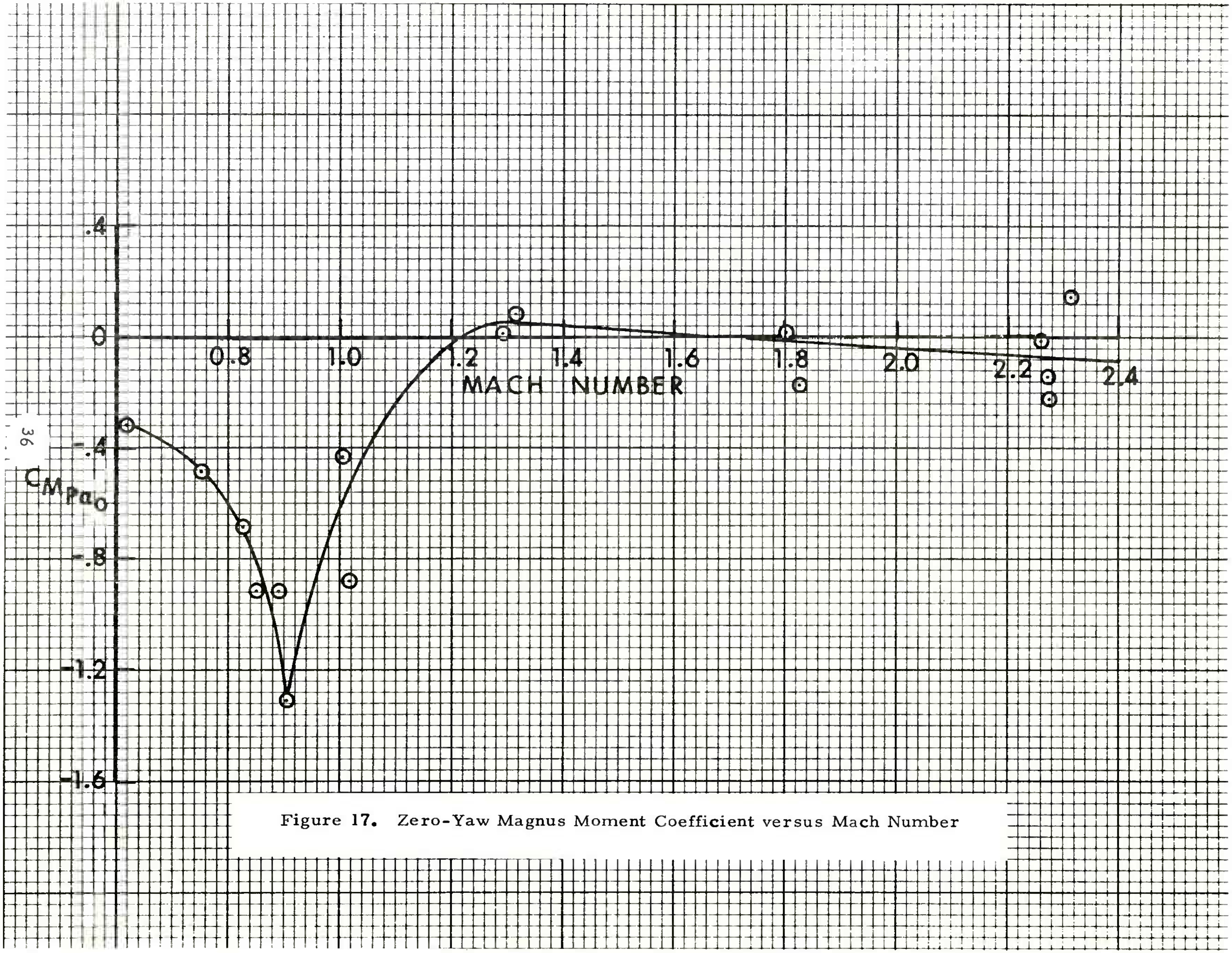

Figure 17. Zero-Yaw Magnus Moment Coefficient versus Mach Number

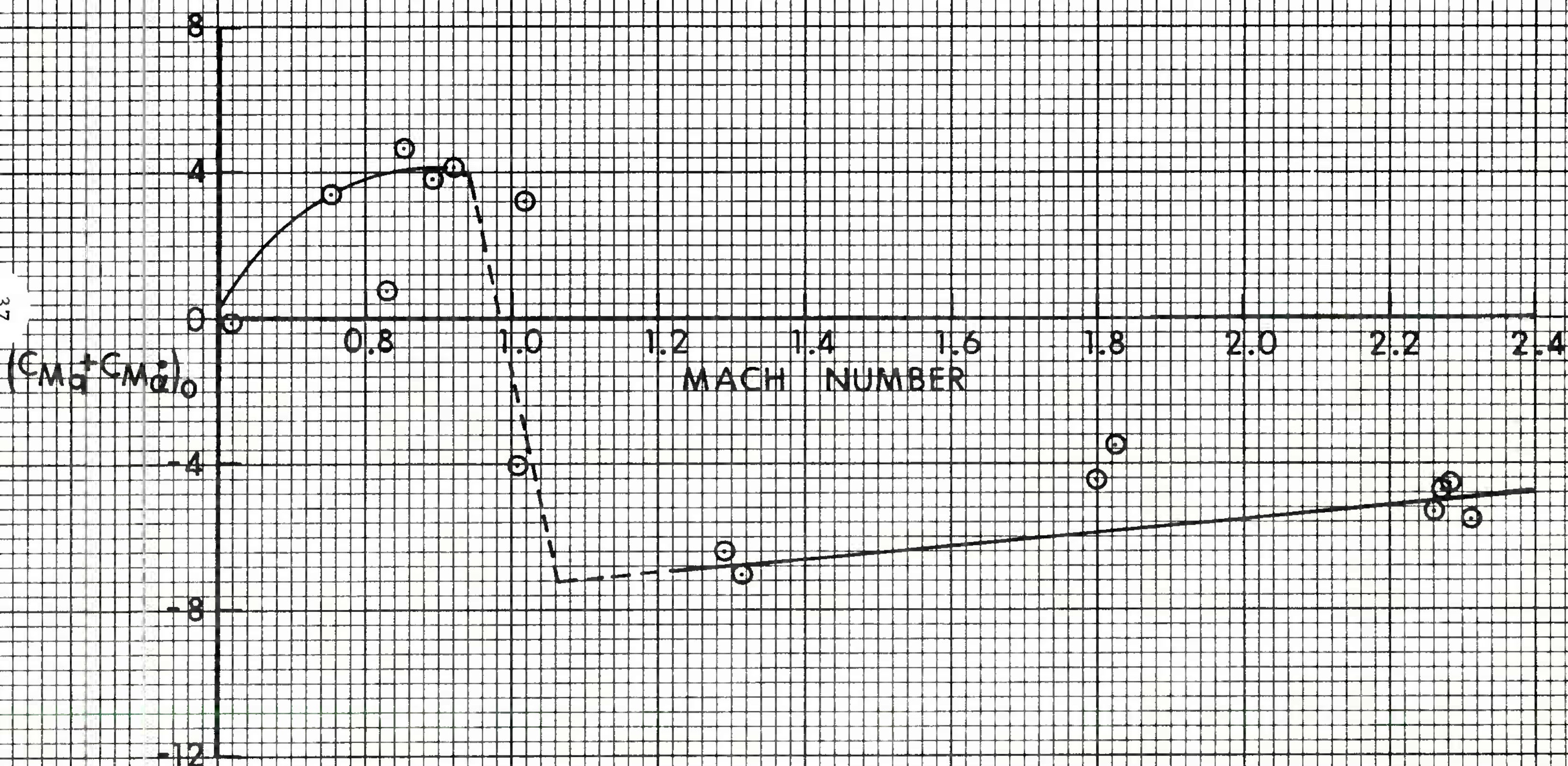

Figure 18. Zero-Yaw Pitch Damping Moment Coefficient Sum versus Mach Number

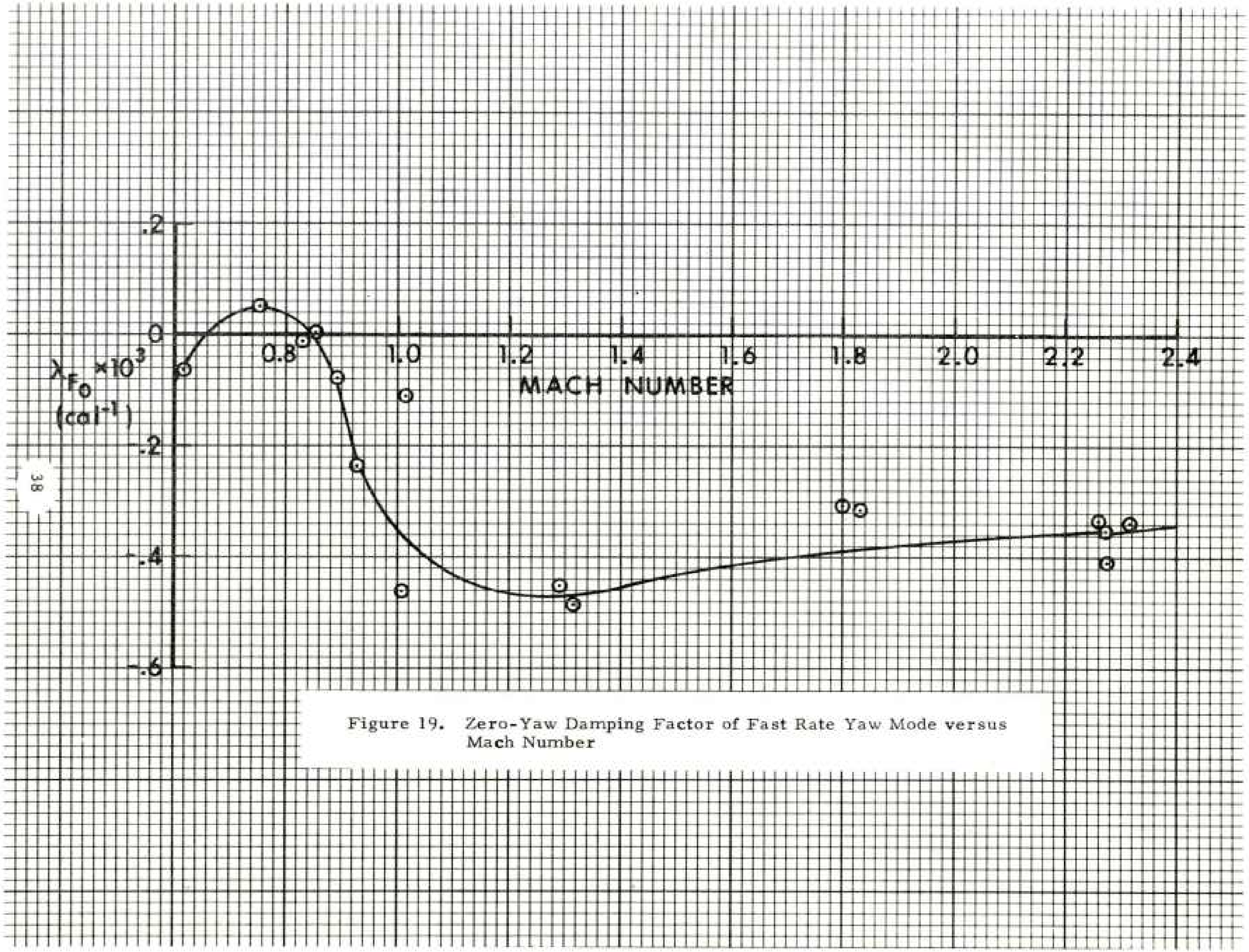

Figure 19. Zero-Yaw Damping Factor of Fast Rate Yaw Mode versus Mach Number

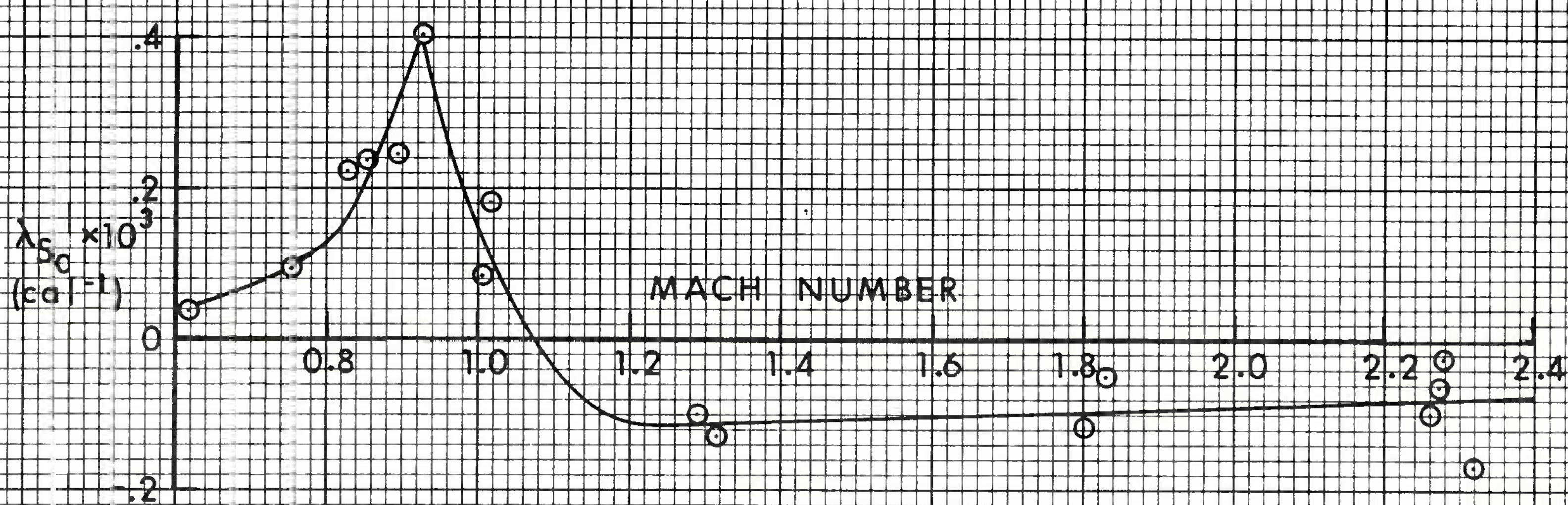

Figure 20. Zero-Yaw Damping Factor of Slow Rate Yaw Mode versus Mach Number

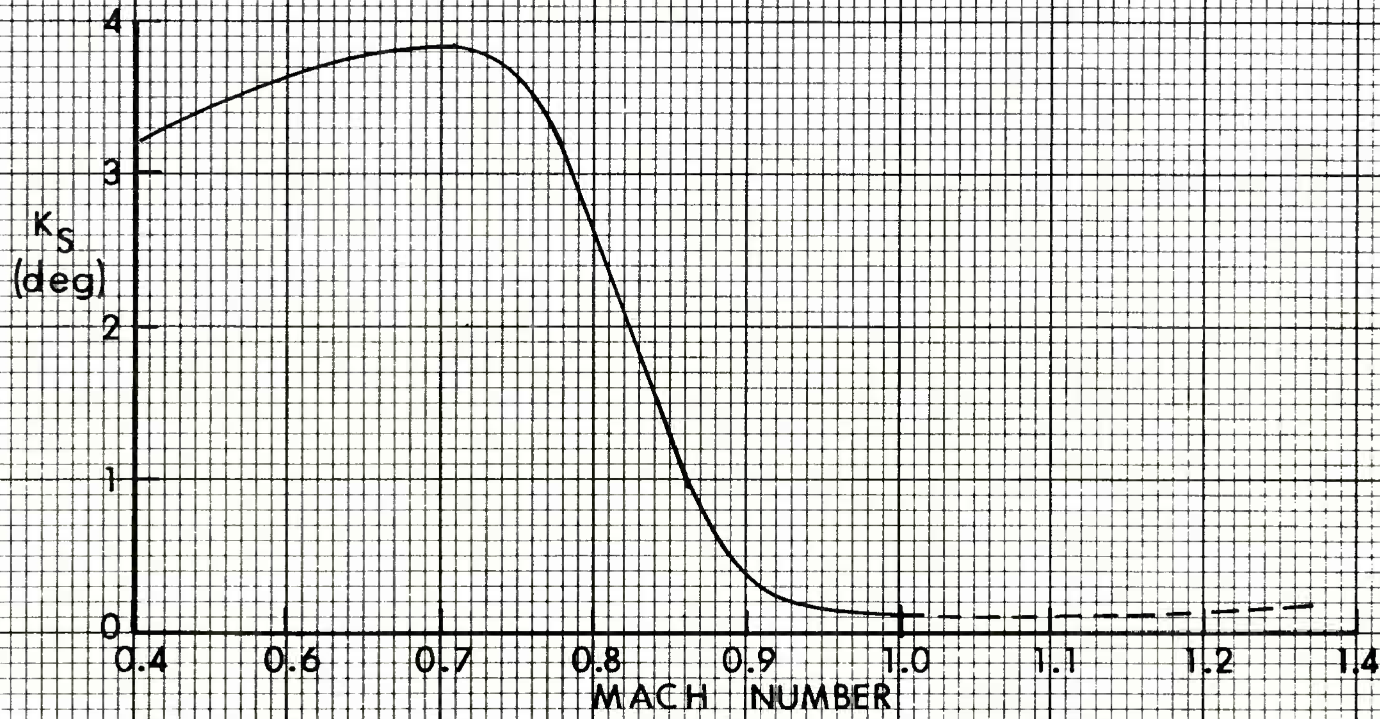

Figure 21. Slow Rate Limit Cycle Yaw versus Mach Number

Table I. Aerodynamic Coefficients of the 30mm, XM788 Projectile

Rd. No.	Mach Number	α_t (deg)	C_D	C_{M_α}	C_{L_α}	$C_{M_{p\alpha}}$	$(C_{M_q} + C_{M_{\dot{\alpha}}})$	CP_N (cal-base)	C_{ℓ_p}
13466	2.316	1.55	.4074	2.40	2.42	.19	-5.72	2.10	-.0089
13465	2.276	1.16	.4068	2.42	2.36	- .19	-4.52	2.12	-.0095
13464	2.271	3.02	.4336	2.35	2.51	.04	-4.93	2.05	---
13463	2.259	3.39	.4408	2.38	2.48	.20	-5.48	2.07	---
13467	1.827	.44	.4527	2.72	2.66	- .17	-3.50	2.11	-.0108
13468	1.800	.54	.4548	2.67	2.27	.04	-4.39	2.23	-.0094
13470	1.314	1.28	.5187	2.75	2.40	.11	-7.06	2.19	-.0118
13469	1.290	1.58	.5225	2.78	2.28	.06	-6.42	2.24	-.0119
13471	1.016	.54	.4479	2.92	2.49	- .88	3.19	2.24	-.0137
13472	1.006	1.08	.4386	2.95	2.12	- .41	-4.06	2.40	-.0145
13474	.925	1.21	.2502	2.93	2.21	-1.30	4.11	2.44	-.0155
13473	.891	2.10	.2334	2.73	2.01	- .88	3.67	2.47	-.0138
13476	.849	2.25	.2288	2.67	1.95	- .87	4.62	2.48	-.0136
13477	.826	7.76	.2924	2.66	1.96	- .10	-1.21	2.43	-.0150
13475	.751	1.62	.2271	2.64	1.60	- .45	3.25	2.70	-.0157
13479	.614	4.37	.2594	2.56	1.78	- .10	- .82	2.50	-.0161

Table II. Flight Motion Parameters of the 30mm, XM788 Projectile

Rd. No.	Mach Number	S_g	S_d	$\lambda_F \times 10^3$ (1/cal)	$\lambda_S \times 10^3$ (1/cal)	K_F	K_S	φ'_F (rad/cal)	φ'_S (rad/cal)
13466	2.316	3.29	.77	-.334	-.189	.0161	.0200	.0421	.0038
13465	2.276	3.25	.29	-.405	-.033	.0116	.0153	.0420	.0039
13464	2.271	3.07	.65	-.331	-.145	.0352	.0399	.0402	.0040
13463	2.259	3.08	.81	-.312	-.195	.0368	.0448	.0405	.0040
13467	1.827	2.98	.46	-.313	-.050	.0050	.0055	.0425	.0043
13468	1.800	3.04	.65	-.303	-.117	.0058	.0068	.0422	.0042
13470	1.314	2.79	.56	-.477	-.141	.0112	.0178	.0407	.0045
13469	1.290	2.76	.52	-.447	-.118	.0145	.0217	.0407	.0046
13471	1.016	2.69	---	-.112	.184	.0067	.0066	.0412	.0047
13472	1.006	2.67	-.15	-.462	.079	.0088	.0158	.0408	.0047
13474	.925	2.56	---	-.240	.397	.0070	.0182	.0397	.0049
13473	.891	2.72	---	-.086	.223	.0197	.0299	.0398	.0046
13476	.849	2.76	---	-.004	.212	.0258	.0284	.0401	.0045
13477	.826	2.76	.79	-.118	-.073	.0911	.0991	.0402	.0045
13475	.751	2.72	---	.049	.108	.0225	.0169	.0401	.0045
13479	.614	2.85	.86	-.095	-.069	.0611	.0454	.0404	.0043

REFERENCES

1. W. F. Braun, "The Free Flight Aerodynamics Range," Ballistic Research Laboratories Report No. 1048, August 1958, AD 202249.

2. E. R. Dickinson, "Physical Measurements of Projectiles," Ballistic Research Laboratories Technical Note No. 874, February 1954, AD 803103.

3. C. H. Murphy, "Data Reduction for the Free Flight Spark Ranges," Ballistic Research Laboratories Report No. 900, February 1954, AD 35833.

4. C. H. Murphy, "The Measurement of Non-Linear Forces and Moments by Means of Free Flight Tests," Ballistic Research Laboratories Report No. 974, February 1956, AD 93521.

5. C. H. Murphy, "Free Flight Motion of Symmetric Missiles," Ballistic Research Laboratories Report No. 1216, July 1963, AD 442757.

6. R. F. Lieske and R. L. McCoy, "Equations of Motion of a Rigid Projectile," Ballistic Research Laboratories Report No. 1244, March 1964, AD 441598.

LIST OF SYMBOLS

a_2 = cubic lift force coefficient

C_2 = cubic static moment coefficient

$\hat{C}_2$ = cubic Magnus moment coefficient

C_D = $\dfrac{\text{Drag Force}}{(1/2)\ \rho\ V^2\ S}$

C_{D_o} = zero yaw drag coefficient

$C_{D_{\delta^2}}$ = quadratic yaw drag coefficient

$C_{D_{\delta^4}}$ = quartic yaw drag coefficient

C_{L_α} = $\dfrac{\text{Lift Force}}{(1/2)\ \rho\ V^2\ S\ \delta}$ Positive coefficient: Force in plane of total angle of attack, α_t, $\perp$ to trajectory in direction of α_t. (α_t directed from trajectory to missile axis.) $\delta = \sin \alpha_t$.

C_{N_α} = $\dfrac{\text{Normal Force}}{(1/2)\ \rho\ V^2\ S\ \delta}$ Positive coefficient: Force in plane of total angle of attack, α_t, $\perp$ to missile axis in direction of α_t.

$$C_{N_\alpha} \cong C_{L_\alpha} + C_D$$

C_{M_α} = $\dfrac{\text{Static Moment}}{(1/2)\ \rho\ V^2\ S\ d\ \delta}$ Positive coefficient: Moment increases angle of attack α_t.

$C_{M_{p\alpha}}$ = $\dfrac{\text{Magnus Moment}}{(1/2)\ \rho\ V^2\ S\ d\ \left(\frac{pd}{V}\right)\delta}$ Positive coefficient: Moment rotates nose $\perp$ to plane of α_t in direction of spin.

$C_{N_{p\alpha}}$ = $\dfrac{\text{Magnus Force}}{(1/2)\,\rho\, V^2\, S\, \left(\frac{pd}{V}\right)\,\delta}$ Negative coefficient: Force acts in direction of 90° rotation of the positive lift force against spin.

For most exterior ballistic uses, where $\dot{\alpha} = q$, $\dot{\beta} = -r$, the definition of the damping moment sum is equivalent to:

$C_{M_q} + C_{M_{\dot{\alpha}}}$ = $\dfrac{\text{Damping Moment}}{(1/2)\,\rho\, V^2\, S\, d\, \left(\frac{q_t d}{V}\right)}$ Positive coefficient: Moment increases angular velocity.

C_{ℓ_p} = $\dfrac{\text{Roll Damping Moment}}{(1/2)\,\rho\, V^2\, S\, d\, \left(\frac{pd}{V}\right)}$ Negative coefficient: Moment decreases rotational velocity.

CP_N = center of pressure of the normal force, positive from base to nose.

α, β = angle of attack, side slip

α_t = $(\alpha^2 + \beta^2)^{1/2} = \sin^{-1}\delta$, total angle of attack

λ_F = fast mode damping rate

λ_S = slow mode damping rate

negative λ indicates damping

ρ = air density

φ'_F = fast mode frequency

φ'_S = slow mode frequency

c. m. = center of mass

d = body diameter of projectile, reference length

d_2 = cubic pitch damping moment coefficient

I_x = axial moment of inertia

I_y	=	transverse moment of inertia
K_F	=	magnitude of the fast yaw mode
K_S	=	magnitude of the slow yaw mode
ℓ	=	length of projectile
m	=	mass of projectile
M	=	Mach number
p	=	roll rate
q, r	=	transverse angular velocities
q_t	=	$(q^2 + r^2)^{1/2}$
R	=	subscript denotes range value
s	=	dimensionless arc length along the trajectory
S	=	$\frac{\pi d^2}{4}$, reference area
S_d	=	dynamic stability factor
S_g	=	gyroscopic stability factor
V	=	velocity of projectile
V_{Muzzle}	=	launch velocity of projectile
$V_{A/C}$	=	aircraft velocity

<u>Effective Squared Yaw Parameters</u>

$\tilde{\delta} \cong K_F^2 + K_S^2$

$$\delta_e^{\,2} = K_F^{\,2} + K_S^{\,2} + \frac{\varphi_F' K_F^{\,2} - \varphi_S' K_S^{\,2}}{\varphi_F' - \varphi_S'}$$

$$\delta_{eF}^{\,2} = K_F^{\,2} + 2\,K_S^{\,2}$$

$$\delta_{eS}^{\,2} = 2\,K_F^{\,2} + K_S^{\,2}$$

$$\delta_{eHT}^{\,2} = \left(\frac{I_Y}{I_X}\right) \frac{(\varphi_F' + \varphi_S')\,(K_S^{\,2} - K_F^{\,2})}{(\varphi_F' - \varphi_S')}$$

$$\delta_{eTH}^{\,2} = \left(\frac{I_X}{I_Y}\right) \frac{(K_F^{\,2}\,\varphi_F'^{\,2} - K_S'^{\,2}\,\varphi_S'^{\,2})}{(\varphi_F'^{\,2} - \varphi_S'^{\,2})}$$

$$\delta_{eHH}^{\,2} = \frac{(\varphi_F' K_S^{\,2} - \varphi_S' K_F^{\,2})}{(\varphi_F' - \varphi_S')}$$

DISTRIBUTION LIST

No. of Copies	Organization
12	Commander Defense Technical Info Center ATTN: DDC-DDA Cameron Station Alexandria, VA 22314
1	Commander US Army Materiel Development & Readiness Command ATTN: DRCDMD-ST 5001 Eisenhower Avenue Alexandria, VA 22333
6	Commander US Army Armament Research & Development Command ATTN: DRDAR-TSS (2 cys) DRDAR-LCA-FF, Mr. S. Wasserman DRDAR-SCS-E, Mr. J. Paz DRDAR-SCF-DA, Mr. J. Spangler Mr. W. Dziwak Dover, NJ 07801
1	Commander US Army Armament Materiel Readiness Command ATTN: DRSAR-LEP-L, Tech Lib Rock Island, IL 61299
1	Director US Army ARRADCOM Benet Weapons Laboratory ATTN: DRDAR-LCB-TL Watervliet, NY 12189
1	Commander US Army Aviation Research & Development Command ATTN: DRSAV-E P.O. Box 209 St. Louis, MO 61366

No. of Copies	Organization
1	Director US Army Air Mobility Research & Development Laboratory Ames Research Center Moffett Field, CA 94035
1	Commander US Army Troop Support & Aviation Materiel Readiness Command ATTN: DRCPM-CO(T), Mr. M. Ryan P.O. Box 209 St. Louis, MO 63166
1	Commander US Army Communications Research & Development Command ATTN: DRDCO-PPA-SA Fort Monmouth, NJ 07703
1	Commander US Army Electronics Research & Development Command Technical Support Activity ATTN: DELSD-L Fort Monmouth, NJ 07703
2	Commander US Army Missile Command ATTN: DRDMI-R DRDMI-YDL Redstone Arsenal, AL 35809
1	Commander US Army Tank Automotive Research & Development Command ATTN: DRDTA-UL Warren, MI 48090
1	Project Manager for Advanced Attack Helicopter, AVRADCOM ATTN: DRCPM-AAH-PM, Mr.J. Romano P.O. Box 209 St. Louis, MO 63166

DISTRIBUTION LIST

No. of Copies	Organization
3	Project Manager for Advanced Attack Helicopter, DARCOM 30mm Ammunition Product Manager Officer ATTN: LTC Dave Logan Mr. A. Cinciosi Dover, NJ 07801
1	Director US Army TRADOC Systems Analysis Activity ATTN: ATAA-SL, Tech Lib White Sands Missile Range NM 88002
3	AFATL/DLDL, G.Winchenbach; K.Cobb; Tech Lib Eglin AFB, FL 32542
1	General Electric Company Armaments Systems Dept. ATTN: Mr. R.H. Whyte Lakeside Avenue Burlington, VT 05401
1	Honeywell, Inc. Defense Systems Division ATTN: Mr. Millivolte 600 Second Street, NE Hopkins, MN 55342
5	Hughes Helicopters Advanced Attack Helicopter ATTN: Ordnance Division Mr. R. Forker Mr. R. Land Mr.J. Waldman Mr. D. Weissenberger Mr. R. W. Bass Centinela and Teale Streets Culver City, CA 90230
1	Skidmore and Shean ATTN: Mr. R. Pfielsticker 1 Oxford Valley Mall Langhorne, PA 19047

Aberdeen Proving Ground

Dir, USAMSAA
ATTN: DRXSY-D
DRXSY-MP, H. Cohen
DRXSY-A, D. O'Neill
T. Coyle
R. Blattner
C. Able
G. Nielsen
DRXSY-G, J. Kramar
DRSXY-R, L. Gentry
DRXSY-S, R. Bailey
M. Carroll
Cdr, USATECOM
ATTN: DRSTE-TO-F
Dir, Wpns Sys Concepts Team
Bldg E3516, EA
ATTN: DRDAR-ACW

USER EVALUATION OF REPORT

Please take a few minutes to answer the questions below; tear out this sheet and return it to Director, US Army Ballistic Research Laboratory, ARRADCOM, ATTN: DRDAR-TSB, Aberdeen Proving Ground, Maryland 21005. Your comments will provide us with information for improving future reports.

1. BRL Report Number____________________________

2. Does this report satisfy a need? (Comment on purpose, related project, or other area of interest for which report will be used.)

____

____

____

3. How, specifically, is the report being used? (Information source, design data or procedure, management procedure, source of ideas, etc.)____________________________

____

____

4. Has the information in this report led to any quantitative savings as far as man-hours/contract dollars saved, operating costs avoided, efficiencies achieved, etc.? If so, please elaborate.

____

____

5. General Comments (Indicate what you think should be changed to make this report and future reports of this type more responsive to your needs, more usable, improve readability, etc.)__________

____

____

____

6. If you would like to be contacted by the personnel who prepared this report to raise specific questions or discuss the topic, please fill in the following information.

Name:____________________________

Telephone Number:____________________________

Organization Address:____________________________

____

____